© 2017. Published by The Company of Biologists Ltd | Development (2017) 144, 1498-1509 doi:10.1242/dev.141630

RESEARCH ARTICLE

Estrogen modulates mesenchyme-epidermis interactions in the adult nipple

Hsing-Jung Wu[1], Ji Won Oh[2,3,4], Dan F. Spandau[5], Sunil Tholpady[6], Jesus Diaz, III[1], Laura J. Schroeder[1], Carlos D. Offutt[1], Adam B. Glick[7], Maksim V. Plikus[2], Sachiko Koyama[1] and John Foley[1,5,*]

ABSTRACT

Maintenance of specialized epidermis requires signals from the underlying mesenchyme; however, the specific pathways involved remain to be identified. By recombining cells from the ventral skin of the *K14-PTHrP* transgenic mice [which overexpress parathyroid hormone-related protein (PTHrP) in their developing epidermis and mammary glands] with those from wild type, we show that transgenic stroma is sufficient to reprogram wild-type keratinocytes into nipple-like epidermis. To identify candidate nipple-specific signaling factors, we compared gene expression signatures of sorted Pdgfrα-positive ventral *K14-PTHrP* and wild-type fibroblasts, identifying differentially expressed transcripts that are involved in WNT, HGF, TGFβ, IGF, BMP, FGF and estrogen signaling. Considering that some of the growth factor pathways are targets for estrogen regulation, we examined the upstream role of this hormone in maintaining the nipple. Ablation of estrogen signaling through ovariectomy produced nipples with abnormally thin epidermis, and we identified TGFβ as a negatively regulated target of estrogen signaling. Estrogen treatment represses Tgfβ1 at the transcript and protein levels in *K14-PTHrP* fibroblasts *in vitro*, while ovariectomy increases *Tgfb1* levels in *K14-PTHrP* ventral skin. Moreover, ectopic delivery of Tgfβ1 protein into nipple connective tissue reduced epidermal proliferation. Taken together, these results show that specialized nipple epidermis is maintained by estrogen-induced repression of TGFβ signaling in the local fibroblasts.

KEY WORDS: Fibroblast, Nipple, Estrogen receptor α, TGFβ, Epidermis

INTRODUCTION

Vertebrates interact with and manipulate their environment by using regions of specialized skin. Epidermis in such specialized skin sites often has distinct stratification patterns, expresses unique differentiation markers and features novel appendages (Billingham and Silvers, 1967). In humans, such sites include nipples, lips, palms, soles, anal and genital skin (Schweizer et al., 1984). Mice share these sites and also feature distinct tail, muzzle and ear skin (Schweizer, 1993). Among these, the nipple stands out for its pivotal role in the mammalian life cycle as a key site for milk transfer from mother to offspring. Thickened and highly proliferative nipple epidermis is uniquely adapted to withstand high mechanical and frictional forces associated with milk delivery (Eastwood et al., 2007; Koyama et al., 2013; Mahler et al., 2004), and it expresses a unique set of keratins and intermediate filament-associated proteins that are largely absent in the trunk epidermis (Eastwood et al., 2007; Mahler et al., 2004). Despite its important function and unique characteristics, little is known about how this epidermal differentiation state is acquired and maintained.

Generally, epithelial specialization is thought to require inductive signals from the underlying connective tissue (Dhouailly et al., 1998). For example, seminal experiments conducted by the Billingham group found that grafts of sole dermis recombined with ear or trunk epidermis produced a thickened and expanded cornified layer, indicating that the mesenchyme specifies the phenotype of the grafted epithelium (Billingham and Silvers, 1967). In other classic experiments, recombination of the palatal epithelium with the cheek connective tissue or vice versa resulted in the *de novo* keratin expression pattern normally associated with the connective tissue type (Mackenzie and Hill, 1981, 1984; Schweizer et al., 1984). Additionally, grafting of the non-palmoplantar epidermal cells onto injured human soles led to epidermis adopting a palmoplantar phenotype, complete with the expression of the site-specific keratin K9 (Yamaguchi, 1999). The lead role of fibroblasts in determining the palmoplantar characteristics of the associated epidermis was further confirmed in follow-up experiments (Yamaguchi, 1999). These classic studies suggest a central role for fibroblasts in determining the anatomical specificity of epidermal cell fate and characteristics.

The inductive and maintenance growth factors produced by site-specific and appendage-specific skin fibroblasts are just starting to be defined (Driskell et al., 2013; Driskell and Watt, 2015; Sriram et al., 2015). Perhaps, the most well-studied cells in this respect are the dermal papilla fibroblasts of the hair follicle, which induce both the formation (Jahoda et al., 1984, 1993; Plikus, 2014; Yang and Cotsarelis, 2010) and regenerative cycling of hair follicles (Chi et al., 2013; Clavel et al., 2012; Enshell-Seijffers et al., 2010; Morgan, 2014; Rendl et al., 2005; Sennett and Rendl, 2012). Dermal papilla fibroblast-specific factors include the fibroblast growth factors Fgf7 and Fgf10 (Chi et al., 2013; Clavel et al., 2012; Enshell-Seijffers et al., 2010; Morgan, 2014; Rendl et al., 2005; Sennett and Rendl, 2012), bone morphogenetic proteins Bmp4 and Bmp6 (Clavel et al., 2012; Rendl et al., 2005, 2008), the BMP antagonist noggin (Botchkarev et al., 1999, 2002; Rendl et al., 2005), transforming growth factor TGFβ2 (Oshimori and Fuchs, 2012) and many others (Morgan, 2014; Rendl et al., 2005; Sennett and Rendl, 2012). Outside of the hair follicle, skin fibroblasts also

[1]Medical Sciences Program, Indiana University School of Medicine, Bloomington, IN 47405, USA. [2]Department of Developmental and Cell Biology, Sue and Bill Gross Stem Cell Research Center, Center for Complex Biological Systems, University of California Irvine, Irvine, CA 92697, USA. [3]Department of Anatomy, School of Medicine, Kyungpook National University, Daegu, 41944, Korea. [4]Biomedical Research Institute, Kyungpook National University Hospital, Daegu, 41944, Korea. [5]Department of Dermatology, Indiana University School of Medicine, Indianapolis, IN 46202, USA. [6]Department of Surgery, Indiana University School of Medicine, Indianapolis, IN 46202, USA. [7]Department of Veterinary and Biomedical Sciences, The Pennsylvania State University, University Park, PA 16802, USA.

*Author for correspondence (jgfoley@indiana.edu)

J.F., 0000-0003-0266-8488

Received 29 June 2016; Accepted 3 March 2017

Development (2017) 144, 1498-1509 doi:10.1242/dev.141630

feature significant specialization and heterogeneity; however, our understanding of their molecular profiles is still rudimentary (Driskell et al., 2013; Driskell and Watt, 2015; Sriram et al., 2015). For instance, recent studies show that papillary (upper) dermis fibroblasts express higher levels of growth factors that control epidermal proliferation and differentiation, whereas those from the reticular (lower) dermis produce high levels of signaling molecules associated with matrix production (Driskell et al., 2013; Driskell and Watt, 2015; Sriram et al., 2015). These findings imply that transcriptional heterogeneity is an intrinsic property related to the developmental history of specific fibroblasts. The notion is further supported by transcriptional profiling studies on skin fibroblasts from different anatomical locations (Chang et al., 2002; Rinn et al., 2006, 2008). Signature profiles of regionally specific skin fibroblasts are in part maintained by their unique homeobox (HOX) gene activities. For example, in human skin, the HOXB genes are expressed in the trunk and non-dermal fibroblasts, whereas HOXD4 and HOXD8 are found exclusively in trunk and proximal leg fibroblasts. Intriguingly, HOXA13 is limited in expression to fibroblasts in distal body sites including hands, feet and foreskin, and its activity is required for the expression of the distal-specific Wingless-Int family growth factor WNT5A (Chang et al., 2002; Rinn et al., 2006, 2008). In mice, differential expression of the HOX gene *Tbx15* between dorsal and ventral skin fibroblasts contributes to the differential skin pigmentation along the sagittal body axis (Candille et al., 2004). Taken together, these findings imply that the developmental history of fibroblasts profoundly impacts upon their inductive and maintenance interactions with the epidermis.

The specific developmental origin of the nipple connective fibroblasts that lie underneath the structure has not been completely established. The mammary gland develops at the interface of what will become dorsal and ventral skin. The mesenchymal cells that lie underneath the mammary line at embryonic day (E)10.5 may be derived from the hypaxial mesoderm (Dhouailly and Oftedal, 2016; Oftedal and Dhouailly, 2013). However, it is not clear whether these or other cells condense around the bud as the primary mammary mesenchyme at E11 to E12.5 (Sakakura, 1987; Sakakura et al., 1987). The differentiation of the mammary mesenchyme is driven in part by parathyroid hormone-related protein (PTHrP; also known as PTHLH) signaling from the developing epithelial cells via PTH/PTHrP receptor (also known as PTH1R) expressed on the stroma. In turn, inductive signaling from these differentiated fibroblasts is required to produce the nipple sheath, which is of distinct evolutionary origin from the gland (Oftedal and Dhouailly, 2013) at E17 (Dunbar et al., 1999; Dunbar and Wysolmerski, 1999; Wysolmerski et al., 1998). Intriguingly, ectopic expression of PTHrP driven by the human keratin 14 promotor in *K14-PTHrP* mice (hereafter KrP mice) dramatically expands the differentiation of the lateral plate mesoderm derivatives to the mammary mesenchyme fate. However, this has minimal impact on cells of the dorsal dermis (Foley et al., 2001). In part, this appears to be the result of increased Bmp4 signaling in the developing ventral skin of the embryo, driving mammary mesenchyme differentiation (Hens et al., 2007). However, other factors such as timing of transgene expression or sensitivity of somatic versus lateral plate-derived mesenchymal cells to PTHrP may be involved (Foley et al., 2001). In the adult female mouse, the ectopic expression of PTHrP results in a hairless skin with a thickened epidermis and complex connective tissue consistent with the nipple (Abdalkhani et al., 2002; Foley et al., 2001, 1998). Whether the fibroblasts that underlie the nipple are simply derived from mammary mesenchyme cells remains to be determined. Nevertheless, during skin development these cells appear to have the capacity to induce and maintain the specialized epidermis that characterizes the structure (Foley et al., 2001; Wu et al., 2015).

In this study, we set out to define the inductive and signaling properties of the specialized fibroblasts from the nipple skin. We established that KrP fibroblasts robustly induce reprogramming of the trunk epidermis towards nipple fate. We also established the unique transcriptional signature of the KrP fibroblasts and evaluated the impact of key pathways identified by that analysis.

RESULTS

Fibroblast-induced reprogramming of trunk keratinocytes into nipple-like epidermis

The instructive capacity of highly specialized nipple fibroblasts has not been established as studies have been limited by the very small size of the appendage in mice. To determine whether nipple fibroblasts have the capacity to reprogram the fate of trunk epidermis, a grafting experiment was carried out using purified cells from ventral skin of neonatal female KrP mice (Wysolmerski et al., 1994), in which close to one quarter of the entire body skin is nipple like (Foley et al., 2001). KrP fibroblasts were recombined with wild-type (WT) neonatal trunk keratinocytes from both dorsal and ventral skin. The resulting grafts were compared to those reconstituted from WT epidermal and dermal cells, as well as the ventral skin of KrP mice (Fig. 1A) (Lichti et al., 2008). When WT keratinocytes and WT fibroblasts were grafted, hairy skin was produced, as previously reported (n=3) (Fig. 1B, left) (Lee et al., 2011; Lichti et al., 2008, 1995, 1993). As expected, reconstitution of KrP neonatal keratinocytes with KrP fibroblasts produced pigmented nipple-like skin with a thickened epidermis and without hair follicles (n=3) (Fig. 1B,C, right panels). Importantly, grafts that recombined WT neonatal keratinocytes with KrP fibroblasts also resulted in pigmented nipple-like skin (n=3) with similar histology to those reconstituted from KrP cells only (Fig. 1B, third panel and 1C, middle panel). As shown on Fig. 1D,E, grafts that contained KrP ventral fibroblasts expressed the nipple epidermis-specific marker keratin K2e (also known as KRT2) and had expanded filaggrin expression, whereas grafts with only WT cells did not. In normal haired mouse skin, melanocytes localize exclusively to hair follicles (Quevedo and Fleischmann, 1980). In contrast, connective tissue of grafts based upon ventral KrP dermal cells contained pigmented cells that we have previously determined to be melanocytes (Abdalkhani et al., 2002) (Fig. 1C, arrows). Thus, dermal cells from KrP ventral skin produce a signaling environment sufficient to induce reprogramming of neonatal trunk keratinocytes towards nipple-like epidermis and formation of pigmented connective tissue.

Pdgfrα is a marker for nipple fibroblasts

Platelet-derived growth factor receptor α (Pdgfrα) was previously reported to be a useful marker for isolating dermal fibroblasts from haired skin (Collins et al., 2011). Here, by using immunofluorescence, we show that Pdgfrα is expressed in nipple fibroblasts, but not in basal keratinocytes in WT ventral skin. It is also expressed in ventral dermis of KrP mice (Fig. 2A). Next, we evaluated Pdgfrα staining along with staining for the fibroblast marker vimentin and found substantial overlap (Fig. 2B). Dual staining for the smooth muscle marker Acta2 and Pdgfrα revealed co-expression in blood vessels, arrector pili muscles, smooth muscle-like cells along the lactiferous duct of the nipple and nests of contractile cells within KrP ventral dermis. These data indicate that Pdgfrα can be used as a marker for isolating specialized fibroblasts

Development (2017) 144, 1498-1509 doi:10.1242/dev.141630

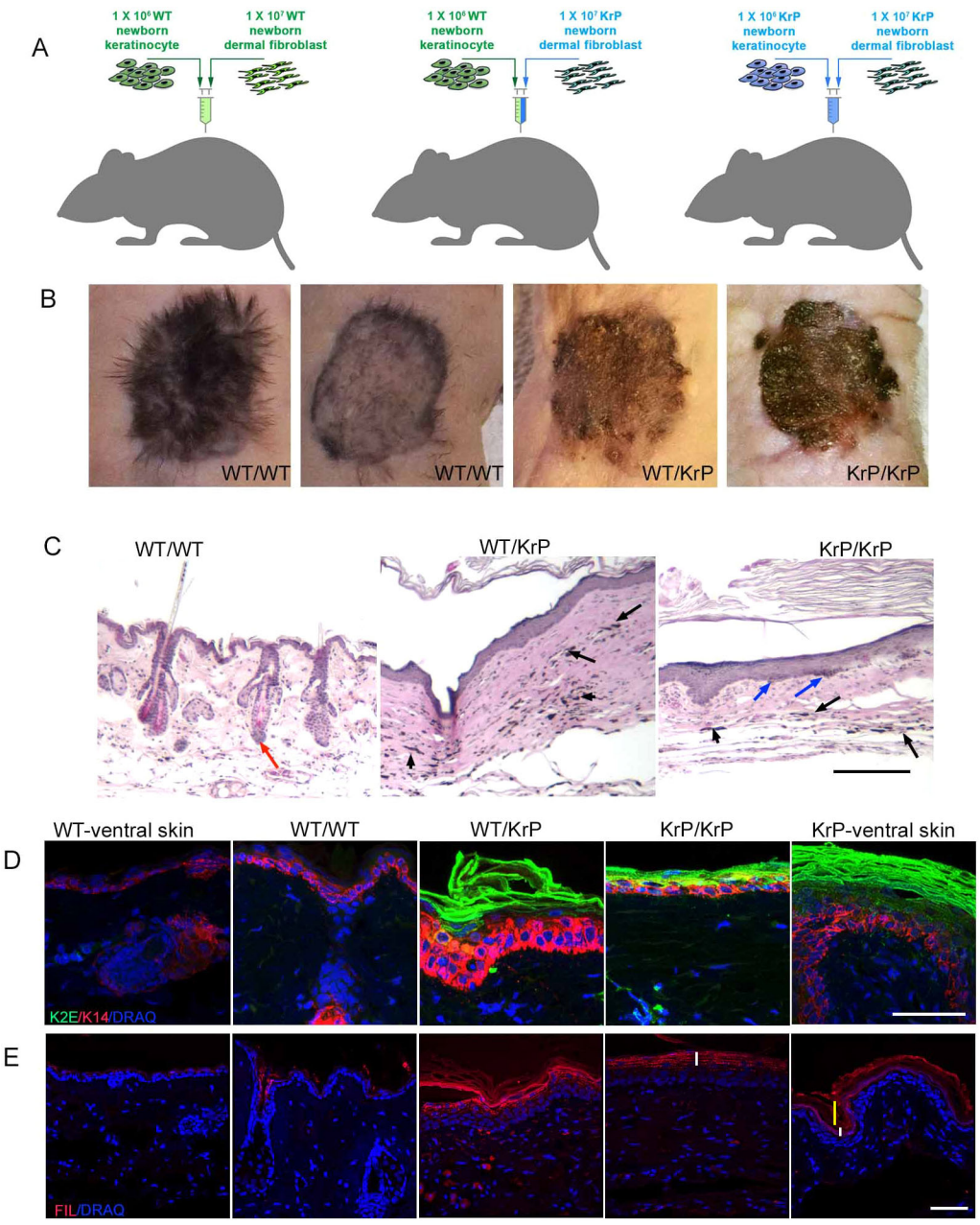

Fig. 1. Fibroblasts from nipple-like skin are sufficient to induce specialized epidermis. (A) Schematic outline of grafting experiment. (B) Hairless pigmented nipple-like skin was present in 3-month-old WT/KrP and KrP/KrP grafts on the dorsum of BALB/c *Foxn1*$^{nu/nu}$ host mice. WT/WT grafts produced pigmented hair, but hair clipping revealed non-pigmented skin underneath. (C) H&E staining of grafts. Black arrows point at pigmented cells in the dermis of KrP/KrP and WT/KrP grafts. Occasionally pigment could be observed in the epidermis of the nipple-like grafts (blue arrows), whereas pigment was mainly confined to hair follicles in WT/WT grafts (red arrow). Scale bar: 400 µm. (D) K2e and K14 immunostaining. WT/KrP and KrP/KrP grafts stain for K2e as does the KrP ventral skin. Scale bar: 50 µm. (E) Filaggrin immunostaining. Multiple suprabasal layers in WT/KrP and KrP/KrP grafts and KrP ventral skin stained for filaggrin, compared to minimal labeling in the WT/WT grafts and intact WT skin. The white vertical bar indicates the granular layer and the yellow bar the cornified layer. Note the cornified layer is lost in the KrP/KrP graft due to antigen retrieval. Scale bar: 50 µm. WT, wild type; KrP, *K14-PTHrP* transgenic mice; K2E, keratin 2e; K14, keratin 14; FIL, filaggrin; DRAQ, nuclei.

from KrP ventral skin; however, the Pdgfrα-positive fraction will also include a few Acta2-positive vascular and muscle cells.

Next, fibroblasts were isolated by fluorescence-activated cell sorting (FACS) from the nipple-like skin of virgin adult female KrP mice and ventral skin of their WT littermates by using an anti-Pdgfrα antibody (which labels the CD140 epitope) (Fig. 3A). To purify cells expressing high amounts of CD140 (the CD140^{hi} population), we set up a dump channel to exclude cells expressing CD31 (endothelial cells), CD117 (melanocytes), CD45 (hematopoietic cells) or CD49f markers (keratinocytes) (Collins et al., 2011). Next, we harvested both WT and KrP RNAs from three distinct cell populations: (1) CD140^{hi} and dump^{-} cells, (2) CD140^{-} and dump^{+} cells, and (3) viable cells expressing none of the markers (Fig. 3B). There was also almost a twofold increase of *Pdgfra* and an elevated expression of *Vim* and *Col1a2* in KrP compared to WT CD140^{+} sorted cells. Next, sorted CD140^{+} or dump^{+} cell populations were transiently cultured for 48 h. While cultured CD140^{+} cells had a branched and elongated spindle-like shape, morphologically similar to a typical fibroblast, dump^{+} cells, were mostly epithelial in appearance (compare Fig. 3C versus Fig. 3D) (Kalluri and Zeisberg, 2006). Thus, we confirmed that Pdgfrα is highly expressed in dermal fibroblasts from the ventral skin of both WT and KrP female mice and that it can be used as a marker for their isolation by sorting.

Microarray profiling reveals a unique gene expression signature of KrP fibroblasts

To identify candidate inductive and maintenance factors present in nipple fibroblasts, we performed microarray-based transcriptome profiling on FACS-sorted CD140^{+} fibroblasts from KrP and WT ventral skin. A total of 123 genes were upregulated and 118 were downregulated in KrP as compared to ventral WT fibroblasts. To identify signaling pathways altered in KrP fibroblasts, differentially expressed genes were subjected to Gene Ontology (GO) analysis and altered signaling of WNT, HGF, TGFβ, IGF, BMP and FGF

Development (2017) 144, 1498-1509 doi:10.1242/dev.141630

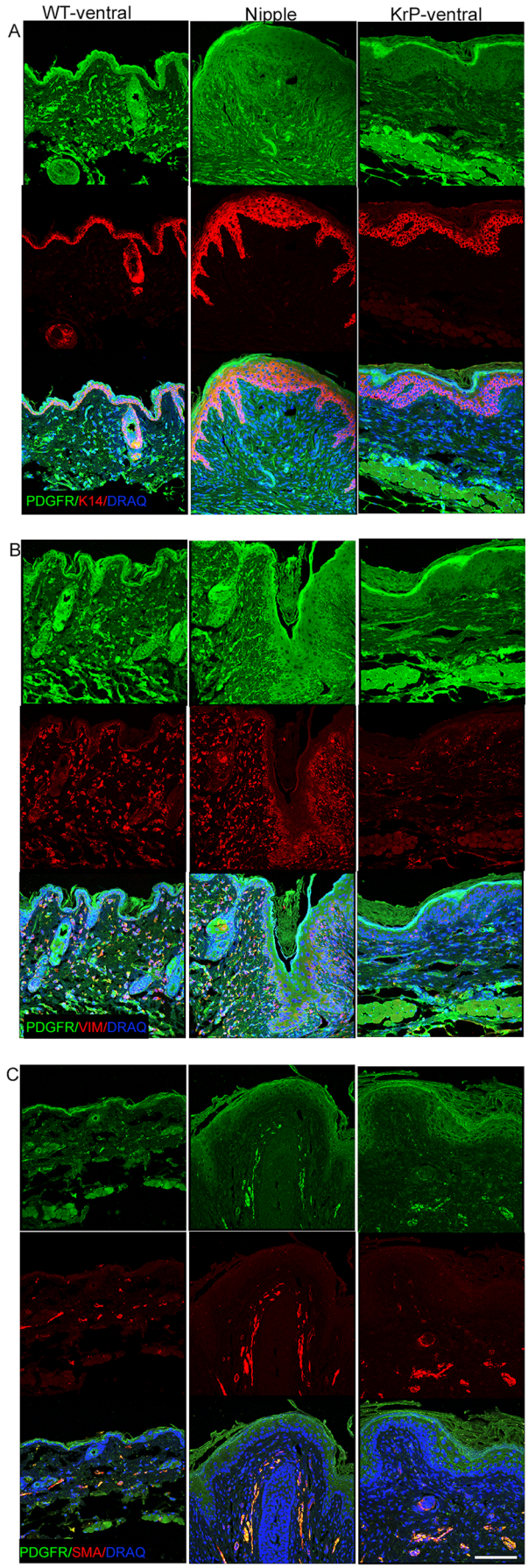

Fig. 2. Pdgfrα expression pattern in ventral skin and nipple tissue. Co-staining of ventral skin from WT mice (left), KrP mice (right) and WT virgin nipple (center) for Pdgfrα (green), and (A) keratin 14 (K14, red), (B) vimentin (Vim, red) or (C) smooth muscle actin (SMA, red). Nuclei were counterstained blue with DRAQ5. Scale bar: 100 µm. The different intensity for Pdgfrα (PDGFR) staining among the sections reflects the use of different antibodies in A and B versus C. The intense labeling of the granular layer in the nipple and KrP samples shown in A and B is likely non-specific.

pathway elements were identified (Fig. 4; Fig. S1). Interestingly, selected extracellular matrix transcripts, including *Col1a1* and *Col1a2*, as well as those from the Timp family of metalloproteinase inhibitors were upregulated, while several metalloproteinase-encoding genes were downregulated in the KrP fibroblasts.

The differential expression of 30 transcripts (20 increased, six decreased and four unchanged in KrP relative to WT fibroblasts), many of which are part of the pathways identified by the Ingenuity and GO term analysis, was largely confirmed by quantitative real-time RT-PCR (qRT-PCR) on sorted fibroblasts as well as micro-dissected virgin WT nipples, WT and intact KrP ventral skin (Figs S2 and S3). We grew both WT and KrP ventral fibroblasts *in vitro* for up to five passages and found signature genes remained differentially regulated in KrP relative to WT ventral fibroblasts (Fig. S4). Overall, differential expression of most genes that comprise the KrP fibroblast signature are known to be consistent in the nipple and stable in primary culture (Rinn et al., 2006, 2008).

Estrogen receptor signaling in fibroblasts maintains nipple structure

Fibroblasts associated with the mammary gland in mice have long been recognized to be responsive to estrogen (Hiremath et al., 2012; Cunha et al., 1997; Wu et al., 2015). Not surprisingly, pregnancy- and lactation-related hormone receptors, including progesterone receptor (*Pgr*), oxytocin receptor (*Oxtr*) and relaxin receptor (*Rxfp1*) were strongly upregulated in the nipple-like KrP fibroblasts as determined by microarray analysis (Fig. 5A). Since both oxytocin and progesterone receptors are regulated by estrogen (Lapidus et al., 1998; Zingg et al., 1998), we next performed qRT-PCR analysis on these hormone receptor-regulated genes using intact ventral skin as well as sorted fibroblasts. Indeed, transcripts for *Esr1*, *Oxtr* and *Pgr* were significantly increased in the WT nipple and KrP nipple-like ventral skin relative to WT non-nipple skin (Fig. 5B). Similar results were also observed for the $CD140^{+}$ sorted KrP fibroblasts (Fig. 5B). Focusing on Esr1, its differential expression between primary cultured fibroblasts from WT versus KrP virgin female ventral skin was confirmed at the protein level by western blotting (Fig. 5C) and in the intact WT nipple by immunofluorescence (Fig. 5D). At the cellular level, nipple fibroblasts had substantial nuclear Esr1 expression (Fig. 5D) (McCormack and Greenwald, 1974). These findings suggest that nipple fibroblasts, including these from the KrP mouse model, maintain stable Esr1 expression and are the target sites for estrogen action.

To further investigate the role of ovarian hormones in the nipple, we ovariectomized (ovexed) pre-pubertal WT and KrP mice, and then harvested nipples and KrP ventral skin between 1.5 and 3 months later. We found that the nipple epidermis in ovexed mice is much thinner than in controls, and the basal layer is less markedly invaginated (Fig. 5E). These changes were accompanied by the diminished expression of the nipple epidermal markers K2e and filaggrin (Fig. 5F; Fig. S5). Moreover, nipple size, which is largely controlled by the extracellular matrix (Wu et al., 2015), was ~30% smaller in the ovexed WT mice as compared to age-matched controls, and specialized nipple connective tissue, typically

Development (2017) 144, 1498-1509 doi:10.1242/dev.141630

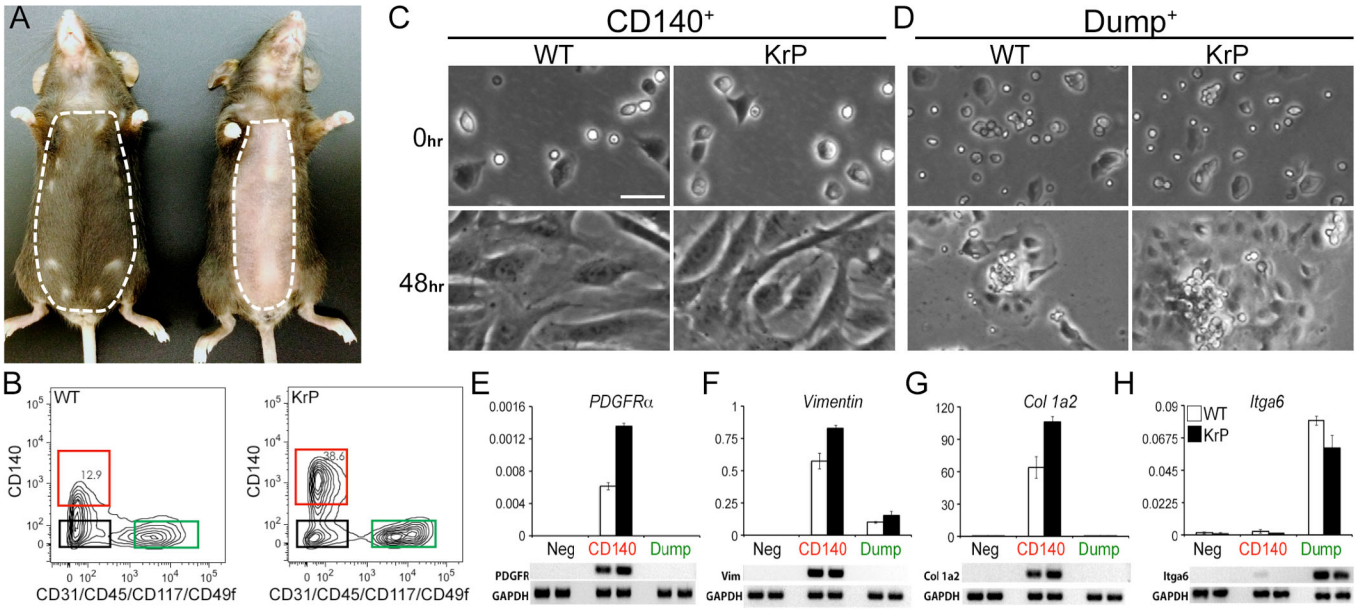

Fig. 3. Pdgfrα labels the mouse nipple fibroblast population. (A) The dotted outline marks the ventral skin in either WT (left) or KrP mice (right) used as the source for fibroblasts. (B) FACS gating strategy used to isolate Pdgfrα$^+$ cells (fibroblasts, red box), dump$^+$ cells (mix of cells marked for CD31$^+$, CD45$^+$, CD117$^+$ or CD49f$^+$; green box) and double-negative Pdgfrα$^-$/Dump$^-$ cells (black box). (C,D) Appearance of sorted Pdgfrα$^+$ cells (C) and dump-channel$^+$ cells (D) immediately after sorting (0 hr) and after culture for 48 h. Only Pdgfrα$^+$ cells display fibroblast morphology after 48 h. Scale bar: 25 µm. (E–H) qRT-PCR for select genes in sorted cell populations (CD140, Pdgfrα$^+$ cells). All target genes were normalized to *Gapdh*. Each bar represents the mean±s.d. of three independent experiments from five mice of each genotype. Bands resulting from qRT-PCR products visualized on 2% agarose gels stained with SYBR Green are shown underneath the graphs.

composed of small tightly packed collagen bundles, was markedly diminished in the ovexed KrP mice (Fig. 5E). Thus, the removal of ovarian hormones, including estrogens, impacts upon both the epidermis and the connective tissue of the nipple.

TGFβ signaling is downregulated in KrP fibroblasts

Upon reviewing the growth factor pathways differentially represented in the KrP fibroblasts as determined by the GO analysis, we found that several of them can be regulated by estrogen in non-nipple tissues (Hewitt et al., 2010; Knabbe et al., 1987; Yokota et al., 2008). Among these is the TGFβ pathway, which has been shown to be inhibited by estrogen signaling components at multiple levels (Cherlet and Murphy, 2007; Colletta et al., 1990), including repression of ligand secretion (Knabbe et al., 1987). This prompted us to further evaluate Tgfβ1 production and signaling in the context of nipple tissue. Indeed, the level of *Tgfb1* transcript was decreased by 50% in sorted KrP fibroblasts as compared to WT ventral skin fibroblasts (Fig. 6A). A similar decrease, of ∼70%, was found in intact WT nipple and KrP skin as compared to ventral WT skin of virgin mice (Fig. 6A). To further validate the reduced TGFβ signaling, we examined the expression levels of phosphorylated Smad2 and Smad3 (pSmad2/3), a specific downstream marker of TGFβ signaling. We show that while nuclear pSmad2/3 expression was observed in most of the ventral skin fibroblasts, fewer nipple fibroblasts were positive (Fig. 6B). Secreted Tgfβ1 protein (as measured by ELISA) was reduced by ∼50% at 48 or 72 h of culture of primary KrP versus WT ventral skin fibroblasts (Fig. 6C), while *Tgfb1* transcript expression remained stably reduced in cultured primary KrP fibroblasts (Fig. 6C) for at least four passages (not shown). As seen by western blotting, the amount of pSmad2/3, but not that of total Smad2/3 protein was reduced in KrP versus WT cultured fibroblasts (Fig. 6D). Taken together, these data suggest that TGFβ signaling is downregulated in nipple fibroblasts.

Estrogen regulates *Tgfb1* transcript levels in KrP fibroblasts

To further establish a functional relationship between estrogen and TGFβ signaling in nipple fibroblasts, we employed primary fibroblast culture in stripped serum Phenol Red-free medium. WT or KrP fibroblasts were treated with 0.5 or 10 nM estradiol for 48 or 72 h, and were then subjected to qRT-PCR analysis. For KrP fibroblasts culture, removal of Phenol Red, a known weak estrogen mimetic, resulted in an increase in the level of *Tgfb1* transcript by 50%, whereas addition of 0.5 nM estradiol lowered *Tgfb1* to the baseline level and 10 nM estradiol reduced it by another 50% (Fig. 6E). We also validated the effect of estradiol on Tgfβ1 at the protein level by ELISA measurements. While the serum-free conditions reduced total Tgfβ1 levels in both WT and KrP fibroblasts, addition of 10 nM of estradiol decreased the amount of protein by 40% only in KrP fibroblast cultures (Fig. 6F). Taken together, these *in vitro* assays demonstrate that *Tgfb1* production is specifically repressed by exogenous estradiol in the KrP fibroblast.

Next, we evaluated TGFβ signaling in an *in vivo* system with altered estrogen signaling, the ovexed KrP mice. As shown in Fig. 6G, *Tgfb1* transcript levels were elevated fourfold in the ventral skin of KrP mice that had been ovexed for 16 weeks, whereas the estrogen-regulated *Esr1* and *Pgr* were reduced by 50% as compared to age-matched samples from intact female KrP mice. As assessed by western blotting, pSmad2/3 protein was elevated in ovexed versus non-ovexed KrP mice (Fig. 6H; Fig. S6), indicating that signaling downstream of TGFβ was elevated in KrP skin under conditions of low estrogen.

Dermal but not epidermal Tgfβ partially shifts nipple features towards those of trunk skin

To initially test the impact of Tgfβ on nipple skin, beads that slowly release Tgfβ1 were implanted into 8-week-old virgin female mouse skin. Beads with or without 0.2 µg of murine recombinant Tgfβ1 were implanted into the nipple dermis of WT mice or ventral skin of

Development (2017) 144, 1498-1509 doi:10.1242/dev.141630

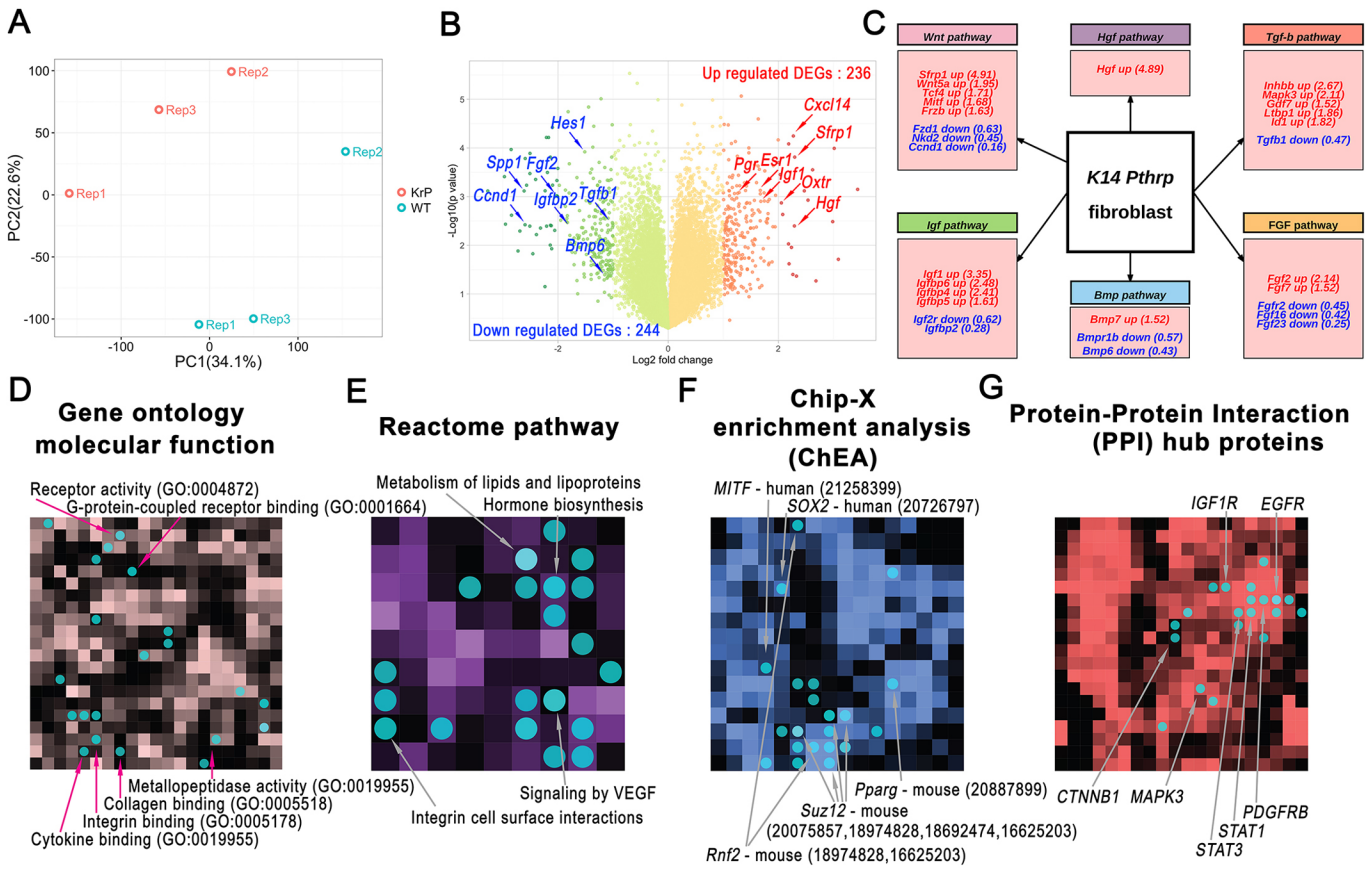

Fig. 4. Bioinformatic comparison of KrP ventral fibroblasts and WT ventral fibroblasts. (A) Principal Component Analysis of KrP (red) versus WT ventral fibroblasts (blue) reveals global gene expression differences between cells of distinct genotypes. Dots represent individual biological replicates. (B) A volcano plot showing the relationship between gene expression fold changes and *P*-values across two genotypes. Red annotations mark differentially expressed genes (DEGs) upregulated in KrP ventral fibroblasts, while blue annotations mark downregulated DEGs. Positions for several up- and down-regulated DEGs on the volcano plot are annotated. (C) Summary of DEGs classified by their signaling pathway identity (WNT, HGF, TGFβ, IGF, BMP or FGF). Red annotations identify DEGs upregulated in KrP ventral fibroblasts, while blue annotations identify downregulated DEGs. For each gene, the KrP versus WT fold-change is provided. (D-G) Network2Canvas analyses for four gene-set libraries: Gene Ontology molecular function (D), Reactome pathway (E), Chip-X enrichment analysis (ChEA) (F), and protein-protein interaction (PPI) hub proteins (G). Each canvas represents a specific gene-set library, where individual squares represent gene lists linked with gene-set library groups (or pathway gene groups). Square brightness is determined by its similarity to its eight neighbors. Each circle (blue) represents top 20 enriched pathways for the KrP versus WT DEGs within the specific gene-set library. Only relevant and statistically significant pathways are annotated here. Full lists of top 20 circles are in Table S2.

KrP mice and their effect was analyzed after 7 days. In contrast to buffer-treated control beads, Tgfβ1-treated beads had a slightly thinner epidermis in WT nipple and KrP skin and led to a thinner papillary dermal layer in the transgenic mice (Fig. 7C). This was accompanied by a significant decrease in epidermal BrdU labeling by ∼50%. In this experiment, Tgfβ1 did not have a measurable impact on WT non-nipple skin (Fig. 7C). To investigate whether Tgfβ1 overexpression could directly influence nipple epidermis, we used doxycycline to induce transgene expression in the *K14-rTA/tetO-TGFb1* mice (Liu et al., 2001), which produces a non-latent porcine form of the TGFβ1 ligand. As shown in Figs S7 and S8, nipple epidermal thickness and BrdU incorporation were similar in transgene-expressing and non-induced double transgenic mice, whereas BrdU incorporation was substantially reduced in the ventral skin of TGFβ1-overexpressing mice. Taken together, these results suggest that overexpression of TGFβ1 within the dermis rather than the epidermis has a greater impact on nipple skin.

DISCUSSION

In this work, we have defined the key molecular and cellular attributes of the fibroblast population that is underneath the specialized epidermis of the murine nipple. First, we showed that fibroblasts from newborn KrP mice induce reprogramming of WT trunk skin keratinocytes towards the nipple fate. Second, we identified the unique gene expression signature of the KrP fibroblasts. Next, we showed that Esr1 signaling is among the major pathways active in KrP fibroblasts and that it acts to suppress TGFβ signaling in KrP fibroblasts *in vitro*. We also present evidence suggesting that the reduced TGFβ pathway activity is essential for endowing nipple skin with its unique characteristics in the adult.

To date, palmoplantar fibroblasts are the most well-defined example of site-specific skin fibroblasts. Their ability to induce reprogramming of keratinocytes into thickened epidermis with a unique keratin expression pattern (Yamaguchi, 1999) has been attributed to several secreted factors. One of them is Dkk1, a soluble inhibitor of canonical WNT signaling (Yamaguchi et al., 2004, 2009, 2008), which also functions to reduce pigmentation of palms and soles by inhibiting melanocyte activity (Yamaguchi et al., 2004, 2009). Another factor is the non-canonical WNT ligand Wnt5a, a putative downstream target of Hoxa13 (Rinn et al., 2006, 2008). Here, we provide the first insight into the signaling network that defines site-specific properties of nipple fibroblasts.

Development (2017) 144, 1498-1509 doi:10.1242/dev.141630

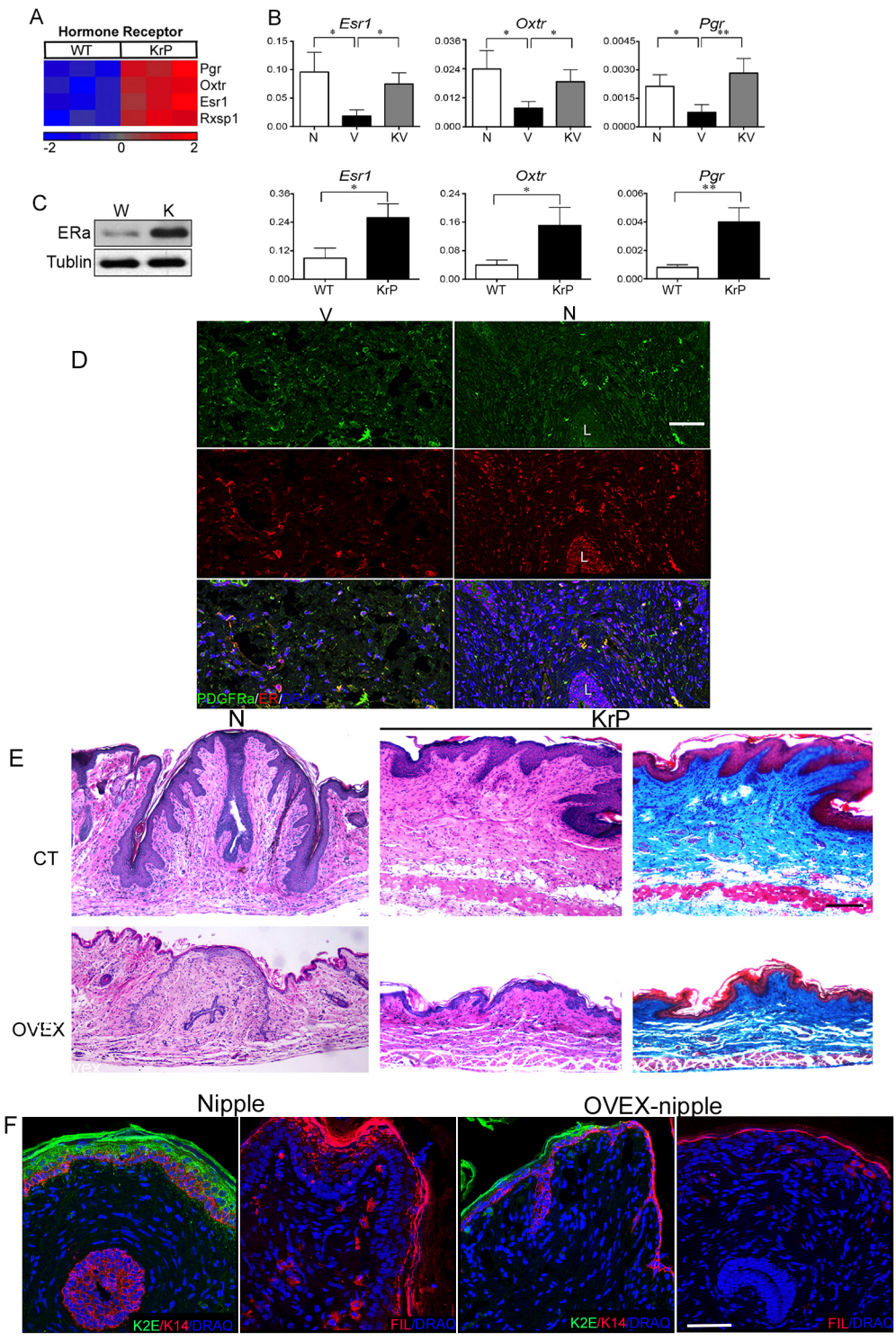

Fig. 5. Estrogen receptor expression and the role of ovarian hormones in the nipple. (A) Heatmap representations of hormone receptor expression in KrP versus WT fibroblasts in three independent experiments. (B) qRT-PCR for receptor gene levels in intact tissues and sorted fibroblasts. N, nipple of WT mouse; V, ventral skin of WT mouse; KV, ventral skin of KrP mouse; WT, sorted WT ventral fibroblast; KrP, sorted KrP fibroblasts. *Esr1*, estrogen receptor α; *Oxtr*, oxytocin receptor; *Pgr*, progesterone receptor. Expression was normalized to *Gapdh* and is expressed as the mean±s.d. of three independent experiments. **P*<0.05, ***P*<0.01. (C) Western blot of cell extracts from cultured KrP and WT fibroblasts probed with anti-estrogen receptor α (ERa) antibody using purified fibroblasts. The same protein extracts used in Fig. 6D were blotted in parallel and the same β-tubulin blot serves as loading control. W, WT ventral fibroblasts; K, KrP fibroblasts. (D) Co-expression patterns of Pdgfrα (green) and ERα (red) in virgin WT mice. Nuclei were counterstained blue with DRAQ5. V, ventral skin; N, nipple; L, lactiferous duct. Scale bar: 60 µm. (E) Histology of WT nipples (N) and KrP ventral skin from ovexed mice. H&E and Masson's trichrome stains demonstrate thinner epidermis and increased size of collagen bundles under ovexed (OVEX) conditions. CT, control. Scale bar: 400 µm. (F) Epidermal marker expression in nipples from ovexed and control mice. Layers of K2e, filaggrin and K14 labeled cells are markedly diminished under ovexed conditions. Scale bar: 50 µm.

Our recombination experiments confirm the leading role of fibroblasts in endowing skin with its regional specificity. We show that KrP stromal cells reprogram WT trunk skin keratinocytes to have nipple-like features, including its stratification pattern and marker profile. It is noteworthy that our KrP stromal cells grafts were pigmented, similar to WT nipple and intact KrP ventral skin (Abdalkhani et al., 2002). This suggests that fibroblasts regulate site-specific skin pigmentation pattern, consistent with the previous experiments on palmoplantar fibroblasts (Yamaguchi et al., 2004, 2009).

Commonly, specialized skin sites in mammals undergo physiological changes in adult life. For instance, palmoplantar skin responds to weight bearing by altering epidermal proliferation dynamics to produce a thick, protective callus (Menz et al., 2007). Perineal skin in the anogenital region of the Old World monkeys can dramatically change in synchrony with the altered reproductive states (VandeBerg et al., 2009). The human nipple and areola skin increases in size and pigmentation during pregnancy and lactation (Javed and Lteif, 2013; Neifert et al., 1990). Estrogen is present at moderate levels during nipple

Development (2017) 144, 1498-1509 doi:10.1242/dev.141630

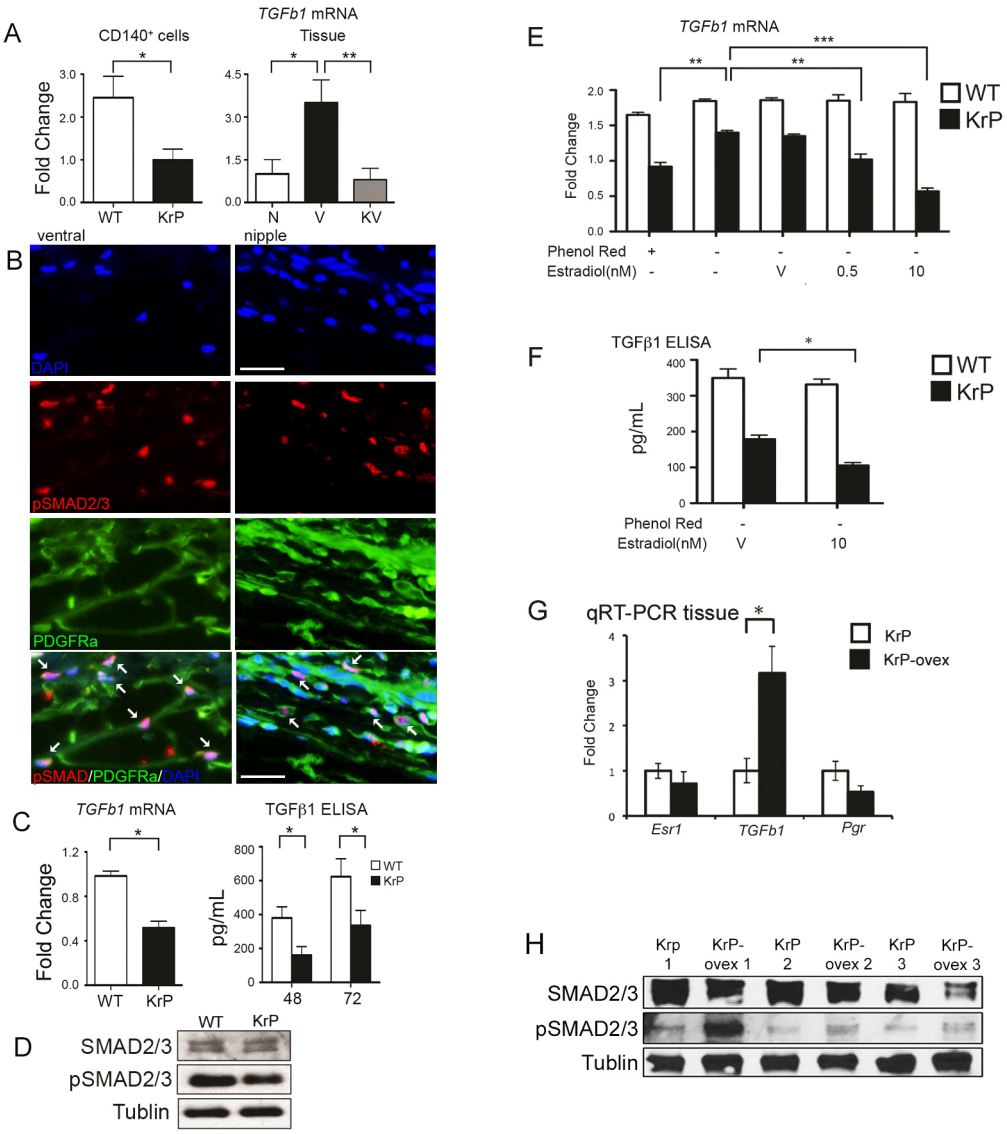

Fig. 6. Estrogen signaling negatively regulates TGFβ signaling in nipple fibroblasts. (A) *Tgfb1* expression in CD140$^+$ sorted fibroblasts and intact tissues. N, nipple of WT mouse; V, ventral skin of WT mouse; KV, ventral skin of KrP mouse. Expression was normalized to *Gapdh* and is expressed as the mean±s.d. of three independent experiments. (B) Co-staining for Pdgfrα (green) and pSmad2/3 (red) of ventral dermis and nipples of virgin WT mouse. Nuclei were counterstained with DAPI (blue). Arrows highlight co-expressing cells. Scale bars: 25 µm. (C) *Tgfb1* expression levels in cultured fibroblasts (measured by qRT-PCR) and secreted levels of Tgfβ1 in culture medium of purified fibroblasts (measured by ELISA). Measurements were collected from three different cultures and performed in triplicate. (D) Western blot of purified fibroblasts probed with antibodies against Smad2/3 and pSmad2/3. The same protein extracts used in Fig. 5C were blotted in parallel and the same β-tubulin blot serves as loading control. (E) Relative *Tgfb1* levels in primary cultured fibroblasts with or without estradiol treatment. Expression of *Tgfb1* was measured by qRT-PCR and normalized to *Gapdh*. Each bar represents the mean±s.d. of three independent experiments. (F) ELISA measurements of secreted Tgfβ1 in culture medium harvested from primary cultured fibroblast with or without estradiol treatment. Each bar represents the mean±s.d. of triplicate cultures within a single experiment. The experiment was repeated twice with similar results. (G) Relative *Esr1*, *Tgfb1* and *Pgr* mRNA levels in ventral skin of ovexed as compared to age-matched control KrP mice. (H) Western blot of extracts from intact ventral tissues from ovexed and control KrP mice probed for Smad2/3 and pSmad2/3. β-tubulin was used as loading control. **P*<0.05, ***P*<0.01, ****P*<0.001.

morphogenesis and Esr1 is dispensable for its formation (Bocchinfuso and Korach, 1997). Our new data from the ovexed mice indicate that estrogen signaling in fibroblasts is necessary for maintaining the thickened epidermis and some connective tissue features of the adult virgin nipple (Fig. 5). The nipple expands during late pregnancy, when estrogen levels peak, and this is accompanied by high levels of nuclear Esr1 in the fibroblasts (Wu et al., 2015). This prompted us to speculate that estrogen likely triggers changes in the signaling environment required for the production and expansion of adult nipple connective tissue, and the maintenance of the unique thickened epidermis. Among several candidate pathways identified in our transcriptomic studies, we focused on the reduction of the TGFβ signaling because it has known effects on fibroblast biology, including regulation of extracellular matrix production, and modulation of growth factor secretion, including keratinocyte growth factor and colony stimulating factor Csf1, which are crucial for the regulation of epidermal proliferation and differentiation (Mauviel, 2009; Szabowski et al., 2000). Consistent with this, we now show that short-term Tgfβ1 bead implantation into the WT nipple and KrP ventral dermis reduces epidermal proliferation, whereas epidermal overexpression of the growth factor fails to do so. One caveat to

Development (2017) 144, 1498-1509 doi:10.1242/dev.141630

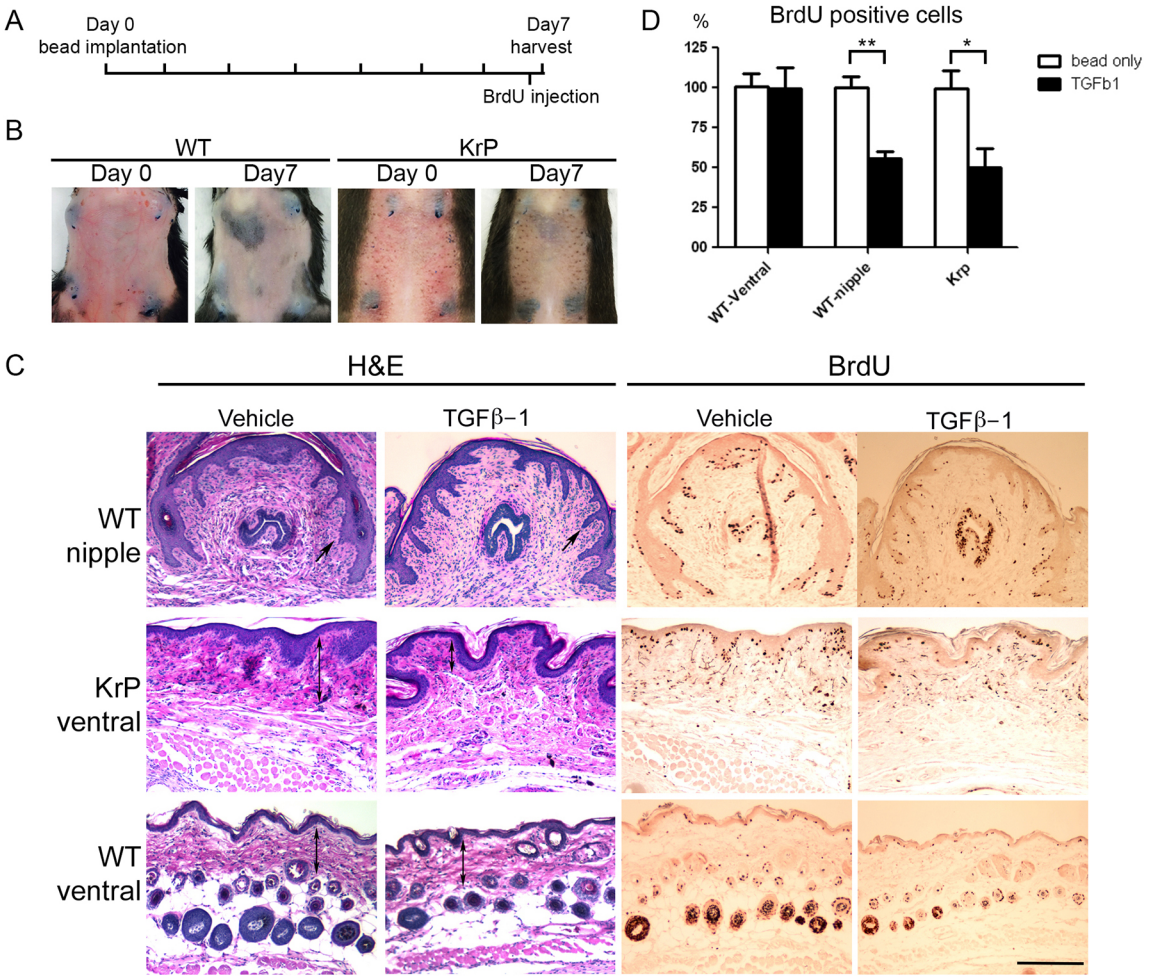

Fig. 7. Sustained dermal activation of TGFβ signaling induces collagen remodeling and epidermal hypoplasia in the nipple. (A) Affi-gel blue beads with or without 0.2 µg of recombinant Tgfβ1 were injected intradermally into KrP ventral skin or WT nipple. Samples were collected at 7 days post-implantation. BrdU was injected 4 h prior to sample collection. (B) Affi-gel blue beads remain at the site of injection 7 days post implantation. (C) Bead-treated samples were stained for H&E and BrdU. Scale bar: 60 µm. (D) Quantification of the percentage of BrdU-positive keratinocytes relative to the length of basal epidermis. *P<0.05, **P<0.01.

these Tgfβ1 studies is that they both used a simple ligand in contrast to the more complex endogenous form, which involves the latency-associated peptide as well as latent TGFβ-binding proteins (Robertson et al., 2015). Nevertheless, these findings imply that at least some aspects of the adult nipple epidermal phenotype can be reversed by ectopic activation of TGFβ signaling, and this appears to be an indirect effect of reduced autocrine TGFβ activity in nipple fibroblasts (Mauviel, 2009). We posit that further studies on some of the signaling pathways revealed here could lead to novel regenerative and tissue engineering approaches for nipple replacement.

MATERIALS AND METHODS

Mice

The *K14-PTHrP* (KrP) transgenic line (Wysolmerski et al., 1994) was maintained by continual breeding against unrelated C57BL/6 mice. WT mice used in this study were either inbred C57BL/6 or littermates of the KrP mice. All animal use was approved by the Indiana University Institutional Animal Care and Use Committee, and was performed in compliance with stipulations of that body. *K14-rTA/tetO-TGFb1* mice were fed 1 g/kg body weight doxycycline chow (Bio-Serve) for 3 weeks to induce transgene expression. Nipples and skin were harvested after BrdU injection (see below). Inbred 1.5- to 3-month-old *Foxn1*$^{nu/nu}$ BALB/c mice (NU/J Jackson Labs) were used as recipients of grafts.

Grafting

Pups derived from the mating of KrP male and WT female mice (1 to 2 days old) were used to isolate keratinocytes and fibroblasts following the protocols developed by Lichti, Yuspa and colleagues (Lichti et al., 2008, 1995, 1993; Weinberg et al., 1993). After genotyping, the ventral skin used was exclusively from KrP-positive female pups whereas the entire trunk skin was used from WT pups. The grafts were composed of 10^7 fibroblasts and 1×10^6-2×10^6 keratinocytes. These were mixed together and applied onto Integra® Dermal Regeneration Template (Integra) and incubated for 1 to 2 h prior to placing on the mouse. The grafting procedure followed the method of Lee et al. (2011). Grafts were harvested 2 to 4 months after the surgery. For each round of grafts, WT epidermal and dermal cells were grafted alone to ensure that hair shafts were not produced, which indicated purity of the cellular preparations (not shown).

Isolation of adult fibroblasts

Primary fibroblasts were isolated as previously described (Lichti et al., 2008; Wu et al., 2015). Briefly, ventral skin from 6- to 8-week-old female virgin WT or KrP mice was carefully dissected to remove mammary glands, and floated on 0.25% trypsin (Gibco Thermo Fisher Scientific) overnight at 4°C. The next day, epidermis was removed, and the remaining tissue was minced and enzymatically digested in a collagenase mixture. The retained cells were then centrifuged at 150 ***g*** for 5 min, and the supernatant was further pelleted at 450 ***g*** for 5 min. Next, pellets from both the 150 ***g*** and 450 ***g*** spin-down were pooled together and washed with Dulbecco's

Development (2017) 144, 1498-1509 doi:10.1242/dev.141630

modified Eagle's medium (DMEM) twice, then centrifuged at 230 ***g*** for 5 min before being strained through a 45 µm mesh. The retained cells were suspended in DMEM and plated at 10^6 cells per 100 mm dish. Additional information on media and chemicals used for this process can be found in the supplementary Materials and Methods.

Flow cytometry

The isolated cells were labeled with anti-mouse CD140a-APC (17-1401-81, eBioscience), anti-mouse CD31-(PECAM-1)-PE (12-0311, eBioscience), anti-mouse CD45-PE (12-045, eBioscience), anti-mouse CD117-(c-kit)-PE (12-1171, eBioscience) and anti-human/anti-mouse CD49f-(Integrin α6)-PE (12-0495, eBioscience) (Collins et al., 2011) (antibodies were used according to the manufacturer's instruction). Meanwhile, 7-aminoactinomycin D (7-AAD) viability staining was performed to exclude dead cells. Cells without antibody labeling and cells with only secondary antibody labeling were used as controls to set the gates. $CD140^+$ cells were collected by using the flow cytometry sorter with FACSDiva software, FACSAria II (BD Biosciences) sorter. FACS analysis was evaluated by FlowJo version X (FlowJo LLC). Re-analysis of the sorted cells indicated a 96-98% purity of $CD140^+$ cells.

Gene expression profiling and microarray studies

Total RNA from $CD140^+$/$dump^-$ dermal fibroblasts from WT or KrP ventral skin of three independent groups, each using five WT and three *K14-PTHrP* female mice were purified as described above. RNA quality was measured by using a 2100 Bioanalyzer (Agilent Technologies), and RNA quantity was accessed by using a Qubit® 2.0 Fluorometer (Q32866, Thermo Fisher Scientific). 20 ng of RNA with RNA integrity number (RIN)≥8 were subjected to reverse transcription and hybridization to Affymetrix Mouse Gene 2.0 ST Arrays. Gene expression data was processed and analyzed using Affymetrix Microarray Analysis Suite Version 5.0 (MAS5.0). Data are available at the Gene Expression Omnibus database under accession GSE87030 (https://www.ncbi.nlm.nih.gov/geo/query/acc.cgi?acc=GSE87030). To identify differentially expressed genes, gene expression was compared between the WT and KrP group in each experiment using a cut-off value of $P<0.05$ in a two-tailed *t*-test and with a fold change of over twofold. Principal Component Analysis was conducted and the Volcano plot produced with the R software package. Differentially expressed genes were then subjected to hierarchical clustering as well as pathway prediction analysis using Network2Canvas (Tan et al., 2013). See Table S1 for individual transcript data.

ELISA for Tgfβ1

5×10^5 WT or KrP primary fibroblasts were seeded in 10 cm dishes in DMEM growth medium (Sigma-Aldrich) supplemented with 10% fetal calf serum (FCS), 100 U/ml penicillin and 100 µg/ml streptomycin overnight for attachment and then serum starved for 12 h. Supernatants were collected at 48 h and 72 h after incubation and centrifuged at 16,000 ***g*** for 10 min at 4°C to remove any debris and stored at −80°C until used. Samples were measured using mouse Tgfβ1 Quantikine ELISA (MB-100B, R&D Systems) following the manufacturer's instruction. Cells were counted after supernatants were harvested, and the Tgfβ1 measurements were normalized to the cell number. Each experiment was carried out in triplicate.

Tgfβ1 agarose bead preparation and implantation

Recombinant mouse Tgfβ1 (7666-MB-005, R&D Systems, Minneapolis, MN) was lyophilized with 0.1% bovine serum albumin (BSA) and stored at −20°C until use. 4 mM of HCl was used to reconstitute recombinant Tgfβ1 to a final concentration of 5-10 µg/ml. 250 µl of Affi-Gel Blue beads (100-200 mesh, Bio-Rad) were soaked in 250 µl of 10 µg/ml Tgfβ1 and incubated at 37°C for 1 h. Beads soaked with lyophilized BSA reconstituted in 4 mM HCl were used as controls. 150 µl of agarose bead suspensions were then injected into the ventral skin of WT and KrP 8-week-old mice using a 22-gauge needle. Sites of agarose bead implantation and the surrounding area of the implantation were harvested after 7 days.

Histology and immunofluorescence

Samples were collected, fixed and sectioned as previously described (Wu et al., 2015). Fluorescence microscope images were obtained with a Nikon NiE (Nikon Instruments) and confocal images were obtained with a Leica TCS SP5 laser-scanning confocal microscope (Leica Microsystems), both at the IUB Light Microscopy Imaging Center of Indiana University. Additional information on antibodies and reagents used for this process can be found in the supplementary Materials and Methods.

Tissue protein extraction and western blotting

Hair-free ventral skin was removed from KrP and KrP ovexed mice. Skin samples were snap-frozen using liquid nitrogen. Samples were digested in a 4% SDS, protease and phosphatase inhibitor solution (1:100, #P8340 and #P0044, Sigma-Aldrich). Mechanical lysis was carried out using an Eppendorf pestle followed by a QIAshredder column. The supernatant protein concentration was measured by using the Pierce BCA protein assay kit (#23227, Thermo Fisher Scientific). Samples were diluted to 0.35 µg/ml, 0.70 µg/ml or 1.40 µg/ml using the 4% SDS solution and a Laemmli Buffer. Whole-cell lysates from primary fibroblasts were prepared by using RIPA buffer, and were simultaneously monitored by blotting for ESR1, pSMAD2/3, SMAD2/3 and tubulin, as a loading control, to determine that increased estrogen receptor levels were correlated with reduced Tgfβ1 signaling *in vitro*. Western blotting was carried out as previously described (Nickerson, 2013). Additional information on antibodies and reagents used for western blotting can be found in the supplementary Materials and Methods.

qRT-PCR

Total RNA was isolated from sorted cells and/or tissues as previously described (Wu et al., 2015) by using an RNeasy mini kit (74104 and 74106, QIAGEN) or an RNeasy micro kit (74004, QIAGEN) with on-column DNase I treatment according to manufacturer's instruction. 1 µg of total RNA was reverse transcribed using SuperScript III First-Strand Synthesis SuperMix Kit (18080400, Thermo Fisher Scientific) to generate cDNA. 40 ng of cDNA was used for qRT-PCR performed on a CFX Connect real-time system (Bio-Rad) using iTaq Universal SYBR Green Supermix (172-5124, Bio-Rad). All results were normalized to the *Gapdh* housekeeping gene using $\Delta\Delta C_T$ method. Primer sequences are available from (Bio-Rad). Analysis was performed on triplicates from samples of cDNA from five animals. Analyses were repeated twice with independently sourced RNA.

BrdU incorporation

Proliferation was assessed by BrdU incorporation through intraperitoneal injection 4 h prior to tissue harvest. A stock solution of 20 mg/ml of 5-bromo-2′-deoxyuridine (BrdU; B5002, Sigma-Aldrich) in 0.9% saline was prepared and stored at −20°C until use. 1 mg of BrdU was injected per 100 g body weight of the mice (Wu et al., 2015).

Statistics

Unless indicated, all *in vivo* data are presented as mean±s.e.m. from at least three replicates from three to six individual animals. All *in vitro* data are presented as mean±s.d. of triplicate measurements of three independent replicates for a single experiment. Experiments were repeated at least twice. Comparisons were evaluated with a Student's *t*-test by using GraphPad Prism, version 5.0 (GraphPad Software); $P<0.05$ was considered to be significant. The genome-wide analysis was carried out using Partek Genomic Suite, version 6.5 (Partek).

Acknowledgements

The microarray studies were carried out using the facilities of the Center for Medical Genomics at Indiana University School of Medicine supported in part by the Indiana Genomics Initiative at Indiana University (INGEN® and the Lilly Endowment, Inc.). We are thankful to Jeanette McClintick for the initial analysis of microarray data sets. We are grateful to Sue Childress for the blocking and serial sectioning of samples. We are grateful to Christiane Hassel at the IU Bloomington Flow Cytometry Core Facility supported by the Indiana CTSI.

Competing interests

The authors declare no competing or financial interests.

Author contributions

H.-J.W., A.B.G., D.F.S., C.D.O., S.T., S.K. and J.F. designed the experiments. H.-J.W., D.F.S., S.T., S.K., C.D.O., L.J.S. and J.F. performed the experiments. H.-J.W., J.F., J.D., M.V.P., S.K., and J.W.O. analyzed the data and H.-J.W., M.V.P., S.K. and J.F. wrote the manuscript.

Funding

This work was supported by a School of Medicine, Indiana University Research Enhancement Grant to J.F. H.-J.W. was supported by the Medical Sciences, Duan and Eunice Dahl Wright Scholarship. M.V.P. is supported by the National Institutes of Health (grants R01-AR067273, R01-AR069653), and grants from the Edward Mallinckrodt Jr. Foundation and Pew Charitable Trusts. Deposited in PMC for release after 12 months.

Data availability

The microarray data reported in this study has been deposited in the Gene Expression Omnibus database under accession number GSE87030 (https://www.ncbi.nlm.nih.gov/geo/query/acc.cgi?acc=GSE87030).

Supplementary information

Supplementary information available online at
http://dev.biologists.org/lookup/doi/10.1242/dev.141630.supplemental

References

Abdalkhani, A., Sellers, R., Gent, J., Wulitich, H., Childress, S., Stein, B., Boissy, R. E., Wysolmerski, J. J. and Foley, J. (2002). Nipple connective tissue and its development: insights from the K14-PTHrP mouse. *Mech. Dev.* **115**, 63-77.

Billingham, R. E. and Silvers, W. K. (1967). Studies on the conservation of epidermal specificities of skin and certain mucosas in adult mammals. *J. Exp. Med.* **125**, 429-446.

Bocchinfuso, W. P. and Korach, K. S. (1997). Mammary gland development and tumorigenesis in estrogen receptor knockout mice. *J. Mammary Gland Biol. Neoplasia* **2**, 323-334.

Botchkarev, V. A., Botchkareva, N. V., Roth, W., Nakamura, M., Chen, L.-H., Herzog, W., Lindner, G., McMahon, J. A., Peters, C., Lauster, R. et al. (1999). Noggin is a mesenchymally derived stimulator of hair-follicle induction. *Nat. Cell Biol.* **1**, 158-164.

Botchkarev, V. A., Botchkareva, N. V., Sharov, A. A., Funa, K., Huber, O. and Gilchrest, B. A. (2002). Modulation of BMP signaling by noggin is required for induction of the secondary (nontylotrich) hair follicles. *J. Invest. Dermatol.* **118**, 3-10.

Candille, S. I., Van Raamsdonk, C. D., Chen, C., Kuijper, S., Chen-Tsai, Y., Russ, A., Meijlink, F. and Barsh, G. S. (2004). Dorsoventral patterning of the mouse coat by Tbx15. *PLoS Biol.* **2**, e3.

Chang, H. Y., Chi, J.-T., Dudoit, S., Bondre, C., van de Rijn, M., Botstein, D. and Brown, P. O. (2002). Diversity, topographic differentiation, and positional memory in human fibroblasts. *Proc. Natl. Acad. Sci. USA* **99**, 12877-12882.

Cherlet, T. and Murphy, L. C. (2007). Estrogen receptors inhibit Smad3 transcriptional activity through Ap-1 transcription factors. *Mol. Cell. Biochem.* **306**, 33-42.

Chi, W., Wu, E. and Morgan, B. A. (2013). Dermal papilla cell number specifies hair size, shape and cycling and its reduction causes follicular decline. *Development* **140**, 1676-1683.

Clavel, C., Grisanti, L., Zemla, R., Rezza, A., Barros, R., Sennett, R., Mazloom, A. R., Chung, C.-Y., Cai, X., Cai, C.-L. et al. (2012). Sox2 in the dermal papilla niche controls hair growth by fine-tuning BMP signaling in differentiating hair shaft progenitors. *Dev. Cell* **23**, 981-994.

Colletta, A. A., Wakefield, L. M., Howell, F. V., van Roozendaal, K. E., Danielpour, D., Ebbs, S. R., Sporn, M. B. and Baum, M. (1990). Anti-oestrogens induce the secretion of active transforming growth factor beta from human fetal fibroblasts. *Br. J. Cancer* **62**, 405-409.

Collins, C. A., Kretzschmar, K. and Watt, F. M. (2011). Reprogramming adult dermis to a neonatal state through epidermal activation of beta-catenin. *Development* **138**, 5189-5199.

Cunha, G. R., Young, P., Hom, Y. K., Cooke, P. S., Taylor, J. A. and Lubahn, D. B. (1997). Elucidation of a role for stromal steroid hormone receptors in mammary gland growth and development using tissue recombinants. *J. Mammary Gland Biol. Neoplasia* **2**, 393-402.

Dhouailly, D. and Oftedal, O. T. (2016). Integument and associated integumentary appendages. In *Kaufmann's Atlas of Mouse Development with Coronal Sections* (ed. R. B. J. Baldock, D. Davidson and G. Morriss-Kay), pp. 147-164. Tokoyo, Japan: Elsevier/Academic Press.

Dhouailly, D., Prin, F., Kanzler, B. and Viallet, J. (1998). Variations of Cutaneous Apendages: regional Specification and Cross-Species Signals. In *Molecular Basis of Epithelial Appendage Morphogenesis* (ed. C. Cheng-Ming), pp. 45-56. Austin, Texas: R.G. Landes Co.

Driskell, R. R. and Watt, F. M. (2015). Understanding fibroblast heterogeneity in the skin. *Trends Cell Biol.* **25**, 92-99.

Driskell, R. R., Lichtenberger, B. M., Hoste, E., Kretzschmar, K., Simons, B. D., Charalambous, M., Ferron, S. R., Herault, Y., Pavlovic, G., Ferguson-Smith, A. C. et al. (2013). Distinct fibroblast lineages determine dermal architecture in skin development and repair. *Nature* **504**, 277-281.

Dunbar, M. E. and Wysolmerski, J. J. (1999). Parathyroid hormone-related protein: a developmental regulatory molecule necessary for mammary gland development. *J. Mammary Gland Biol. Neoplasia* **4**, 21-34.

Dunbar, M. E., Dann, P. R., Robinson, G. W., Hennighausen, L., Zhang, J. P. and Wysolmerski, J. J. (1999). Parathyroid hormone-related protein signaling is necessary for sexual dimorphism during embryonic mammary development. *Development* **126**, 3485-3493.

Eastwood, J., Offutt, C., Menon, K., Keel, M., Hrncirova, P., Novotny, M. V., Arnold, R. and Foley, J. (2007). Identification of markers for nipple epidermis: changes in expression during pregnancy and lactation. *Differentiation* **75**, 75-83.

Enshell-Seijffers, D., Lindon, C., Kashiwagi, M. and Morgan, B. A. (2010). beta-catenin activity in the dermal papilla regulates morphogenesis and regeneration of hair. *Dev. Cell* **18**, 633-642.

Foley, J., Longely, B. J., Wysolmerski, J. J., Dreyer, B. E., Broadus, A. E. and Philbrick, W. M. (1998). PTHrP regulates epidermal differentiation in adult mice. *J. Invest. Dermatol.* **111**, 1122-1128.

Foley, J., Dann, P., Hong, J., Cosgrove, J., Dreyer, B., Rimm, D., Dunbar, M., Philbrick, W. and Wysolmerski, J. (2001). Parathyroid hormone-related protein maintains mammary epithelial fate and triggers nipple skin differentiation during embryonic breast development. *Development* **128**, 513-525.

Hens, J. R., Dann, P., Zhang, J.-P., Harris, S., Robinson, G. W. and Wysolmerski, J. (2007). BMP4 and PTHrP interact to stimulate ductal outgrowth during embryonic mammary development and to inhibit hair follicle induction. *Development* **134**, 1221-1230.

Hewitt, S. C., Li, Y., Li, L. and Korach, K. S. (2010). Estrogen-mediated regulation of Igf1 transcription and uterine growth involves direct binding of estrogen receptor alpha to estrogen-responsive elements. *J. Biol. Chem.* **285**, 2676-2685.

Hiremath, M., Dann, P., Fischer, J., Butterworth, D., Boras-Granic, K., Hens, J., Van Houten, J., Shi, W. and Wysolmerski, J. (2012). Parathyroid hormone-related protein activates Wnt signaling to specify the embryonic mammary mesenchyme. *Development* **139**, 4239-4249.

Jahoda, C. A. B., Horne, K. A. and Oliver, R. F. (1984). Induction of hair growth by implantation of cultured dermal papilla cells. *Nature* **311**, 560-562.

Jahoda, C. A. B., Reynolds, A. J. and Oliver, R. F. (1993). Induction of hair growth in ear wounds by cultured dermal papilla cells. *J. Invest. Dermatol.* **101**, 584-590.

Javed, A. and Lteif, A. (2013). Development of the human breast. *Semin. Plastic Surg.* **27**, 5-12.

Kalluri, R. and Zeisberg, M. (2006). Fibroblasts in cancer. *Nat. Rev. Cancer* **6**, 392-401.

Knabbe, C., Lippman, M. E., Wakefield, L. M., Flanders, K. C., Kasid, A., Derynck, R. and Dickson, R. B. (1987). Evidence that transforming growth factor-beta is a hormonally regulated negative growth factor in human breast cancer cells. *Cell* **48**, 417-428.

Koyama, S., Wu, H.-J., Easwaran, T., Thopady, S. and Foley, J. (2013). The nipple: a simple intersection of mammary gland and integument, but focal point of organ function. *J. Mammary Gland Biol. Neoplasia* **18**, 121-131.

Lapidus, R. G., Nass, S. J. and Davidson, N. E. (1998). The loss of estrogen and progesterone receptor gene expression in human breast cancer. *J. Mammary Gland Biol. Neoplasia* **3**, 85-94.

Lee, L. F., Jiang, T. X., Garner, W. and Chuong, C.-M. (2011). A simplified procedure to reconstitute hair-producing skin. *Tissue Eng. C* **17**, 391-400.

Lichti, U., Weinberg, W. C., Goodman, L., Ledbetter, S., Dooley, T., Morgan, D. and Yuspa, S. H. (1993). In vivo regulation of murine hair growth: insights from grafting defined cell populations onto nude mice. *J. Invest. Dermatol.* **101**, 124S-129S.

Lichti, U., Scandurro, A. B., Kartasova, T., Rubin, J. S., LaRochelle, W. and Yuspa, S. H. (1995). Hair follicle development and hair growth from defined cell populations grafted onto nude mice. *J. Invest. Dermatol.* **104**, 43S-44S.

Lichti, U., Anders, J. and Yuspa, S. H. (2008). Isolation and short-term culture of primary keratinocytes, hair follicle populations and dermal cells from newborn mice and keratinocytes from adult mice for in vitro analysis and for grafting to immunodeficient mice. *Nat. Protoc.* **3**, 799-810.

Liu, X., Alexander, V., Vijayachandra, K., Bhogte, E., Diamond, I. and Glick, A. (2001). Conditional epidermal expression of TGFbeta 1 blocks neonatal lethality but causes a reversible hyperplasia and alopecia. *Proc. Natl. Acad. Sci. USA* **98**, 9139-9144.

Mackenzie, I. C. and Hill, M. W. (1981). Maintenance of regionally specific patterns of cell proliferation and differentiation in transplanted skin and oral mucosa. *Cell Tissue Res.* **219**, 597-607.

Mackenzie, I. C. and Hill, M. W. (1984). Connective tissue influences on patterns of epithelial architecture and keratinization in skin and oral mucosa of the adult mouse. *Cell Tissue Res.* **235**, 551-559.

Mahler, B., Gocken, T., Brojan, M., Childress, S., Spandau, D. F. and Foley, J. (2004). Keratin 2e: a marker for murine nipple epidermis. *Cells Tissues Organs* **176**, 169-177.
Mauviel, A. (2009). Transforming growth factor-beta signaling in skin: stromal to epithelial cross-talk. *J. Invest. Dermatol.* **129**, 7-9.
McCormack, J. T. and Greenwald, G. S. (1974). Progesterone and oestradiol-17beta concentrations in the peripheral plasma during pregnancy in the mouse. *J. Endocrinol.* **62**, 101-107.
Menz, H. B., Zammit, G. V. and Munteanu, S. E. (2007). Plantar pressures are higher under callused regions of the foot in older people. *Clin. Exp. Dermatol.* **32**, 375-380.
Morgan, B. A. (2014). The dermal papilla: an instructive niche for epithelial stem and progenitor cells in development and regeneration of the hair follicle. *Cold Spring Harb. Perspect. Med.* **4**, a015180.
Neifert, M., DeMarzo, S., Seacat, J., Young, D., Leff, M. and Orleans, M. (1990). The influence of breast surgery, breast appearance, and pregnancy-induced breast changes on lactation sufficiency as measured by infant weight gain. *Birth* **17**, 31-38.
Nickerson, N. (2013). Autocrine-derived epidermal growth factor receptor ligands contribute to recruitment of tumor-associated macrophage and growth of basal breast cancer cells in vivo. *Oncol. Res.* **20**, 303-317.
Oftedal, O. T. and Dhouailly, D. (2013). Evo-devo of the mammary gland. *J. Mammary Gland Biol. Neoplasia* **18**, 105-120.
Oshimori, N. and Fuchs, E. (2012). Paracrine TGF-beta signaling counterbalances BMP-mediated repression in hair follicle stem cell activation. *Cell Stem Cell* **10**, 63-75.
Plikus, M. V. (2014). At the dawn of hair research - testing the limits of hair follicle regeneration. *Exp. Dermatol.* **23**, 314-315.
Quevedo, W. C., Jr and Fleischmann, R. D. (1980). Developmental biology of mammalian melanocytes. *J. Invest. Dermatol.* **75**, 116-120.
Rendl, M., Lewis, L. and Fuchs, E. (2005). Molecular dissection of mesenchymal-epithelial interactions in the hair follicle. *PLoS Biol.* **3**, e331.
Rendl, M., Polak, L. and Fuchs, E. (2008). BMP signaling in dermal papilla cells is required for their hair follicle-inductive properties. *Genes Dev.* **22**, 543-557.
Rinn, J. L., Bondre, C., Gladstone, H. B., Brown, P. O. and Chang, H. Y. (2006). Anatomic demarcation by positional variation in fibroblast gene expression programs. *PLoS Genet.* **2**, e119.
Rinn, J. L., Wang, J. K., Allen, N., Brugmann, S. A., Mikels, A. J., Liu, H., Ridky, T. W., Stadler, H. S., Nusse, R., Helms, J. A. et al. (2008). A dermal HOX transcriptional program regulates site-specific epidermal fate. *Genes Dev.* **22**, 303-307.
Robertson, I. B., Horiguchi, M., Zilberberg, L., Dabovic, B., Hadjiolova, K. and Rifkin, D. B. (2015). Latent TGF-beta-binding proteins. *Matrix Biol.* **47**, 44-53.
Sakakura, T. (1987). Mammary embryogenesis. In *The Mammary Gland: Development, Regulation, and Function* (ed. M. C. Neville and C. W. Daniel), pp. 37-66. New York: Plenum Press.
Sakakura, T., Kusano, I., Kusakabe, M., Inaguma, Y. and Nishizuka, Y. (1987). Biology of mammary fat pad in fetal mouse: capacity to support development of various fetal epithelia in vivo. *Development* **100**, 421-430.
Schweizer, J. (1993). Murine epidermal keratins. In *Molecular Biology of the Skin: The Keratinocyte* (ed. M. Darmon and M. L. Blumenberg), pp. 33-78. San Diego: Academic Press.
Schweizer, J., Winter, H., Hill, M. W. and Mackenzie, I. C. (1984). The keratin polypeptide patterns in heterotypically recombined epithelia of skin and mucosa of adult mouse. *Differentiation* **26**, 144-153.
Sennett, R. and Rendl, M. (2012). Mesenchymal-epithelial interactions during hair follicle morphogenesis and cycling. *Semin. Cell Dev. Biol.* **23**, 917-927.
Sriram, G., Bigliardi, P. L. and Bigliardi-Qi, M. (2015). Fibroblast heterogeneity and its implications for engineering organotypic skin models in vitro. *Eur. J. Cell Biol.*
Szabowski, A., Maas-Szabowski, N., Andrecht, S., Kolbus, A., Schorpp-Kistner, M., Fusenig, N. E. and Angel, P. (2000). c-Jun and JunB antagonistically control cytokine-regulated mesenchymal-epidermal interaction in skin. *Cell* **103**, 745-755.
Tan, C. M., Chen, E. Y., Dannenfelser, R., Clark, N. R. and Ma'ayan, A. (2013). Network2Canvas: network visualization on a canvas with enrichment analysis. *Bioinformatics* **29**, 1872-1878.
VandeBerg, J. L., Williams-Blangero, S. and Tardif, S. D. (2009). *The Baboon in Biomedical Research*. New York: Springer.
Weinberg, W. C., Goodman, L. V., George, C., Morgan, D. L., Ledbetter, S., Yuspa, S. H. and Lichti, U. (1993). Reconstitution of hair follicle development in vivo: determination of follicle formation, hair growth, and hair quality by dermal cells. *J. Invest. Dermatol.* **100**, 229-236.
Wu, H.-J., Easwaran, T., Offutt, C. D., Elgar, R. L., Spandau, D. F., Koyama, S. and Foley, J. (2015). Expansion of specialized epidermis induced by hormonal state and mechanical strain. *Mech. Dev.* **136**, 73-86.
Wysolmerski, J. J., Broadus, A. E., Zhou, J., Fuchs, E., Milstone, L. M. and Philbrick, W. M. (1994). Overexpression of parathyroid hormone-related protein in the skin of transgenic mice interferes with hair follicle development. *Proc. Natl. Acad. Sci. USA* **91**, 1133-1137.
Wysolmerski, J. J., Philbrick, W. M., Dunbar, M. E., Lanske, B., Kronenberg, H. and Broadus, A. E. (1998). Rescue of the parathyroid hormone-related protein knockout mouse demonstrates that parathyroid hormone-related protein is essential for mammary gland development. *Development* **125**, 1285-1294.
Yamaguchi, (1999). Regulation of keratin 9 in nonpalmoplantar keratinocytes by palmoplantar fibroblasts through epithelial-mesenchymal interactions. *J. Invest. Dermatol.* **112**, 483-488.
Yamaguchi, Y., Itami, S., Watabe, H., Yasumoto, K., Abdel-Malek, Z. A., Kubo, T., Rouzaud, F., Tanemura, A., Yoshikawa, K. and Hearing, V. J. (2004). Mesenchymal-epithelial interactions in the skin: increased expression of dickkopf1 by palmoplantar fibroblasts inhibits melanocyte growth and differentiation. *J. Cell Biol.* **165**, 275-285.
Yamaguchi, Y., Passeron, T., Hoashi, T., Watabe, H., Rouzaud, F., Yasumoto, K.-I., Hara, T., Tohyama, C., Katayama, I., Miki, T. et al. (2008). Dickkopf 1 (DKK1) regulates skin pigmentation and thickness by affecting Wnt/beta-catenin signaling in keratinocytes. *FASEB J.* **22**, 1009-1020.
Yamaguchi, Y., Morita, A., Maeda, A. and Hearing, V. J. (2009). Regulation of skin pigmentation and thickness by Dickkopf 1 (DKK1). *J. Investig. Dermatol. Symp. Proc.* **14**, 73-75.
Yang, C.-C. and Cotsarelis, G. (2010). Review of hair follicle dermal cells. *J. Dermatol. Sci.* **57**, 2-11.
Yokota, T., Oritani, K., Garrett, K. P., Kouro, T., Nishida, M., Takahashi, I., Ichii, M., Satoh, Y., Kincade, P. W. and Kanakura, Y. (2008). Soluble frizzled-related protein 1 is estrogen inducible in bone marrow stromal cells and suppresses the earliest events in lymphopoiesis. *J. Immunol.* **181**, 6061-6072.
Zingg, H. H., Grazzini, E., Breton, C., Larcher, A., Rozen, F., Russo, C., Guillon, G. and Mouillac, B. (1998). Genomic and non-genomic mechanisms of oxytocin receptor regulation. *Adv. Exp. Med. Biol.* **449**, 287-295.

Supplemental Methods

Isolation of adult fibroblasts

The collagenase solution contained 1.25 mg/ml Collagenase type I (Gibco Thermo Fisher Scientific, Waltham, MA), 0.5 mg/ml Collagenase type II (Worthington Biochemical Co., Lakewood, NJ), 0.5 mg/ml Collagenase type IV (Sigma-Aldrich, St. Louis, MO), and 50 U/ml DNase I (Worthington Biochemical Co., Lakewood, NJ) in DMEM media at 37°C for one hour. The preparations were then passed through blunt-end needles several times to mechanically dissociate dermis before filtering the mixture through a 70 μm strainer.

Note that the ventral dermis of WT mice would contain a very small number of nipple fibroblasts.

Histology and immunofluorescence

Samples were collected, fixed and sectioned as previously described (Wu et al., 2015). The following primary antibodies against the following proteins were used: vimentin (mouse monoclonal, ab28028, Abcam, Cambridge MA), smooth muscle actin 1:50 (mouse monoclonal, A2547, Sigma-Aldrich, St. Louis MO), cytokeratin 2e 1:500 (mouse monoclonal 10R-C166a, Fitzgerald, Acton, MA), Keratin 14 (rabbit polyclonal, 905301, BioLegend, San Diego, CA), filaggrin 1:5,000 (rabbit polyclonal, 905801, BioLegend, San Diego, CA), Pdgfrα 1:200 (goat polyclonal, AF1062, R&D systems, Minneapolis MN and C-9 Santa Cruz Biotechnology, Dallas, TX), Esr1 (rabbit polyclonal, HC-20, Santa Cruz Biotechnology, Dallas, TX), Smad2/3 (rabbit polyclonal, FL-425, Santa Cruz Biotechnology, Dallas, TX),

pSmad2/3 1:200 (goat polyclonal, sc-11769, Santa Cruz Biotechnology, Dallas, TX). Secondary antibodies were used at 1:200 to 1:500 dilution (Jackson Immuno Research Laboratories Inc., West Grove, PA), including Alexa-Fluor 488 or 647- conjugated goat anti-rabbit or anti-mouse IgG. Nucleus staining was conducted using DAPI (D1306, Thermo Fisher Scientific, Waltham, MA) or Draq5 (62251, Thermo Fisher Scientific, Waltham, MA).

Western Blotting

The following primary antibodies were used: ERa (rabbit polyclonal, HC-20, Santa Cruz Biotechnology, Dallas, TX), Smad2/3 (rabbit polyclonal, FL-425, Santa Cruz Biotechnology, Dallas, TX), pSmad2/3 (sc-11769R, Santa Cruz Biotechnology, Dallas, TX). For the tissue analysis the following antibodies were used: β-tubulin 1:125 (mouse monoclonal, E7-s, Developmental Studies Hybridoma Bank, Iowa City IA), p-Smad2/3 (Ser 423/425) 1:100 (rabbit polyclonal, sc-11769, Santa Cruz Biotechnology, Dallas, TX), Smad2/3 (C-8) 1:200 (mouse monoclonal, sc-133098, Santa Cruz Biotechnology, Dallas, TX).

Supplementary Tables

Supplementary table S1. Microarray gene expression data and analysis. Data are generated from sorted Pdgfrα-positive ventral KrP and WT fibroblasts. Tab 1, raw gene expression data; tab 2, list of up-regulated genes; tab 3, list of down-regulated genes; tab 4, select signaling pathway genes; tab 5, reference signaling pathway gene list.

Click here to Download Table S1

Supplementary table S2. Differential gene expression analysis on Pdgfrα-positive ventral KrP and WT fibroblasts using Network2Canvas platform. Individual tabs contains lists of enriched terms within given gene networks.

Click here to Download Table S2

Supplemental Figures

Supplementfig1

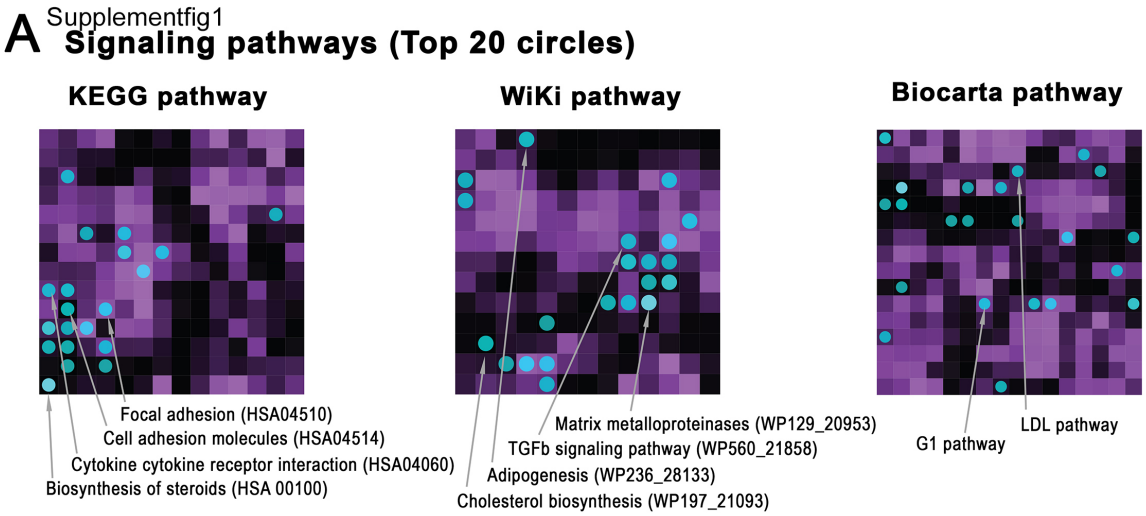

Supplemental figure S1. Network2Canvas analysis of KrP *vs.* WT ventral fibroblasts for seven gene-set libraries. Signaling pathways **(A),** Transcription **(B),** Kinase enrichment analysis **(C),** and Gene ontology and Cancer cell line encyclopedia **(D).** Each canvas represents a specific gene-set library, where each square represents a gene list linked with a gene-set library group. Square brightness is determined by its similarity to its eight neighbors. Each circle (blue) represents top 20 enriched pathways using KrP *vs.* WT DEGs within specific gene set library. Only relevant and statistically significant pathways are selectively annotated. Also see Supplementary tables S1 and S2.

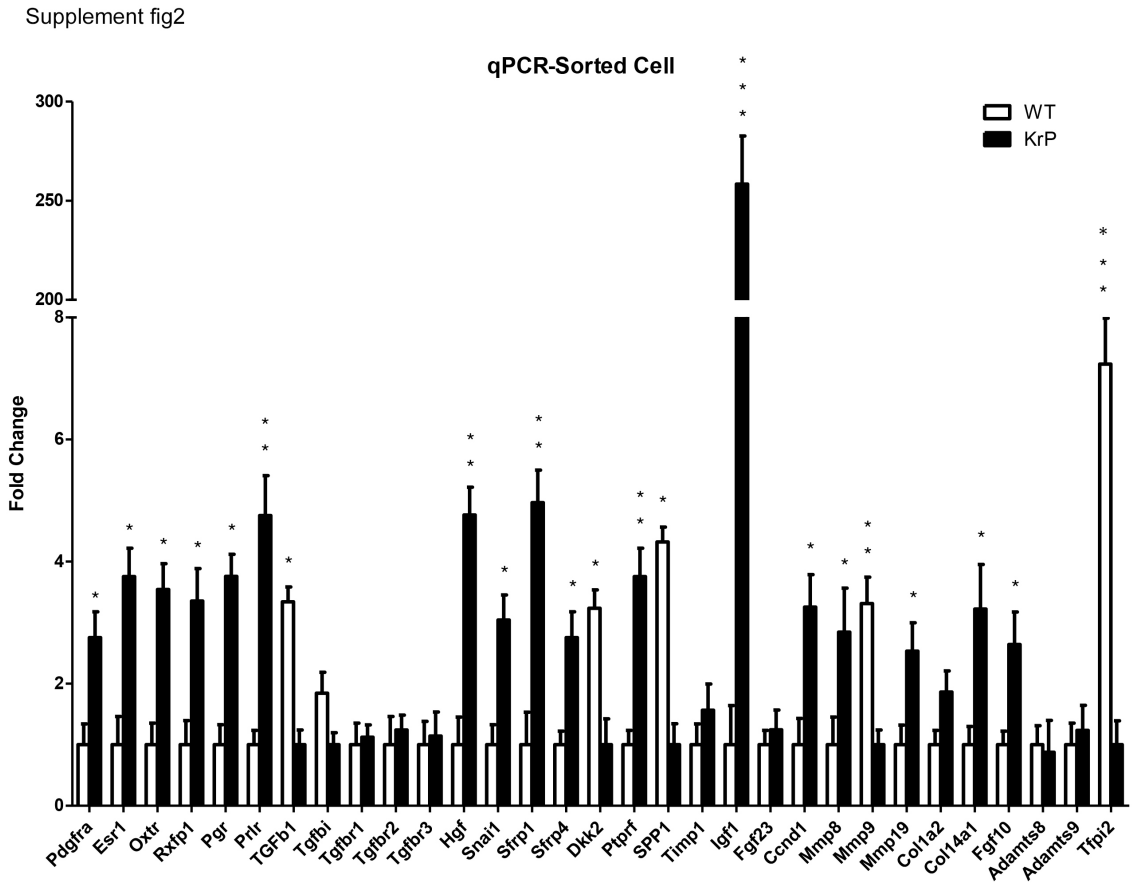

Supplemental Figure S2. Confirmation of select differentially expressed genes by qRT-PCR using RNA from sorted cells. The differential expression of 30 transcripts (20 increased, 6 decreased and 4 unchanged in KrP relative to WT fibroblasts), many of which are part of the pathways identified by the Ingenuity and GO term analysis, was confirmed by qRT-PCR (Fig. S2). Of the transcripts evaluated, all with the exception of *Fgf23, Adamts9,* and *Timp1* exhibited substantial expression level differences. In addition, levels of *Ccd1* on qRT-PCR were opposite of the microarray data. Cells were sorted as in Figure 3**.** Relative mRNA levels of selected genes where the average lower expressing set of samples were arbitrarily set to 1. Each bar represents the average of three independent experiments (±s.d.). *P < 0.05, **P < 0.01, ***P < 0.001.

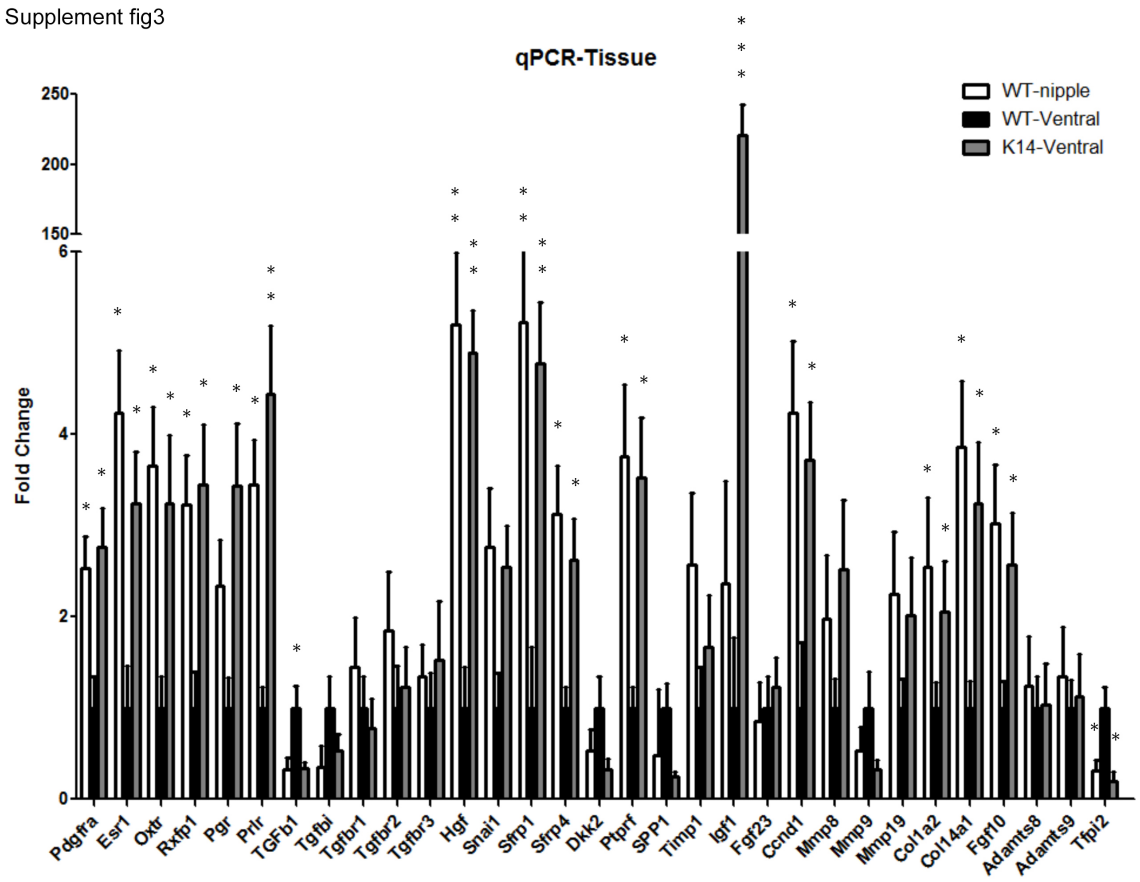

Supplemental Figure S3. Confirmation of select differentially expressed genes by qRT-PCR using RNA from intact tissues. To determine if the differential gene expression pattern of KrP fibroblasts was representative of the intact nipple, we validated it by qRT-PCR on RNA from the micro dissected nipples WT and KrP ventral skin. Indeed, all transcripts with the exception of the genes noted in figure 2 , were either elevated or reduced in the WT nipple as compared to WT non-nipple ventral skin in accordance with the KrP-to-WT fibroblasts differences (Fig. S3). In addition, *Igf1* expression was substantially lower (by ~100 fold) in the intact WT nipple as compared to KrP fibroblasts, or intact KrP ventral skin (Fig. S2, S3). Relative mRNA levels of selected genes where the WT ventral skin samples were arbitrarily set to 1. Each bar represents the average of three independent experiments (±s.d.). *P < 0.05, **P < 0.01, ***P < 0.001.

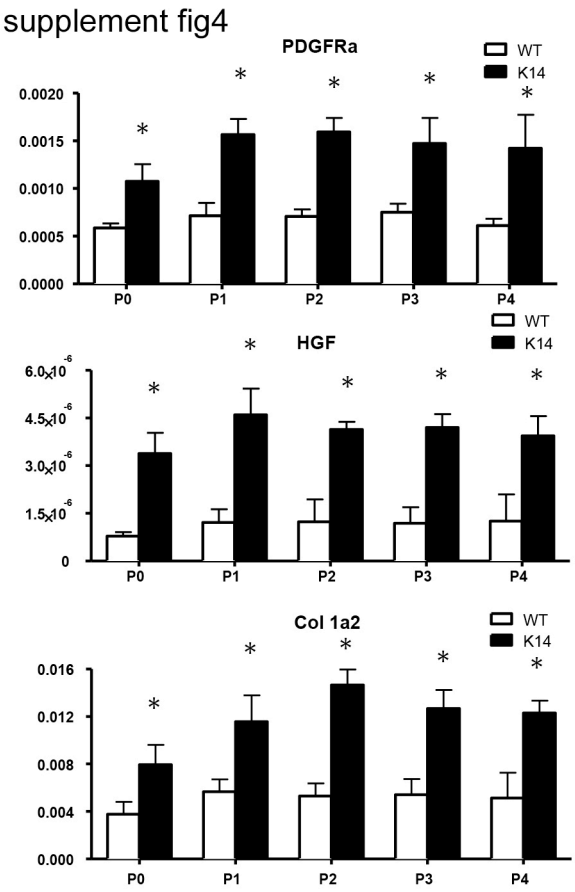

Supplemental Figure S4. Differential gene expression is maintained *in vitro*.

(A-D) To determine if the nipple fibroblast signature was stable in culture, we grew both WT and KrP ventral fibroblasts *in vitro* for up to 5 passages. We evaluated three signature transcripts (*Col1a*, *Pdgfrα* and *Hgf)* and found they remained differentially regulated in KrP relative to WT ventral fibroblasts, suggesting that some gene expression studies can be performed with cells grown *in vitro*. Relative mRNA levels in primary cultured fibroblasts at various passages. Expression of these transcripts was measured by qRT-PCR and normalized to *Gapdh* using absolute method. Each bar represents the average of three independent experiments (±s.d.). *P < 0.05.

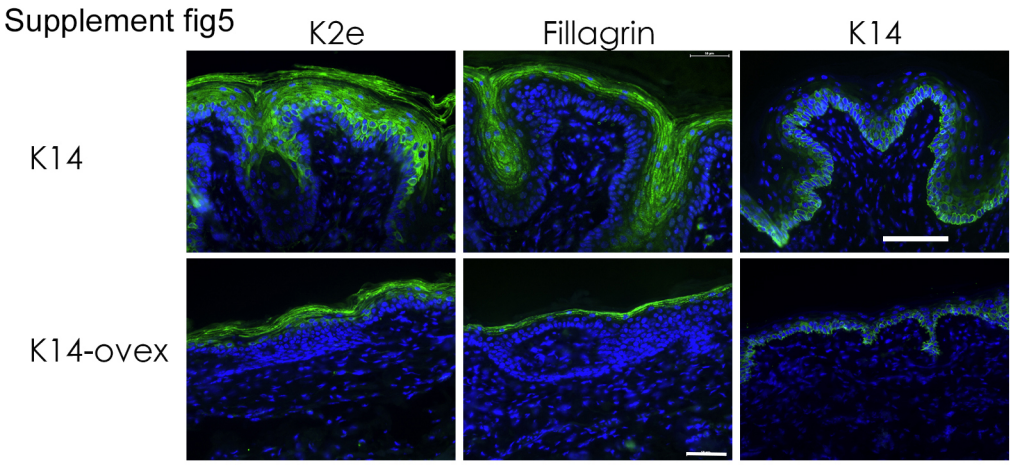

Supplemental Figure S5. Differentiation marker expression in ovexed KrP skin. Samples are indicated on the left and antibody used on the top. Layers of K2e, filaggrin and K14 antibody labeled cells are markedly diminished in ovexed mice. . Scale bar: 50μm

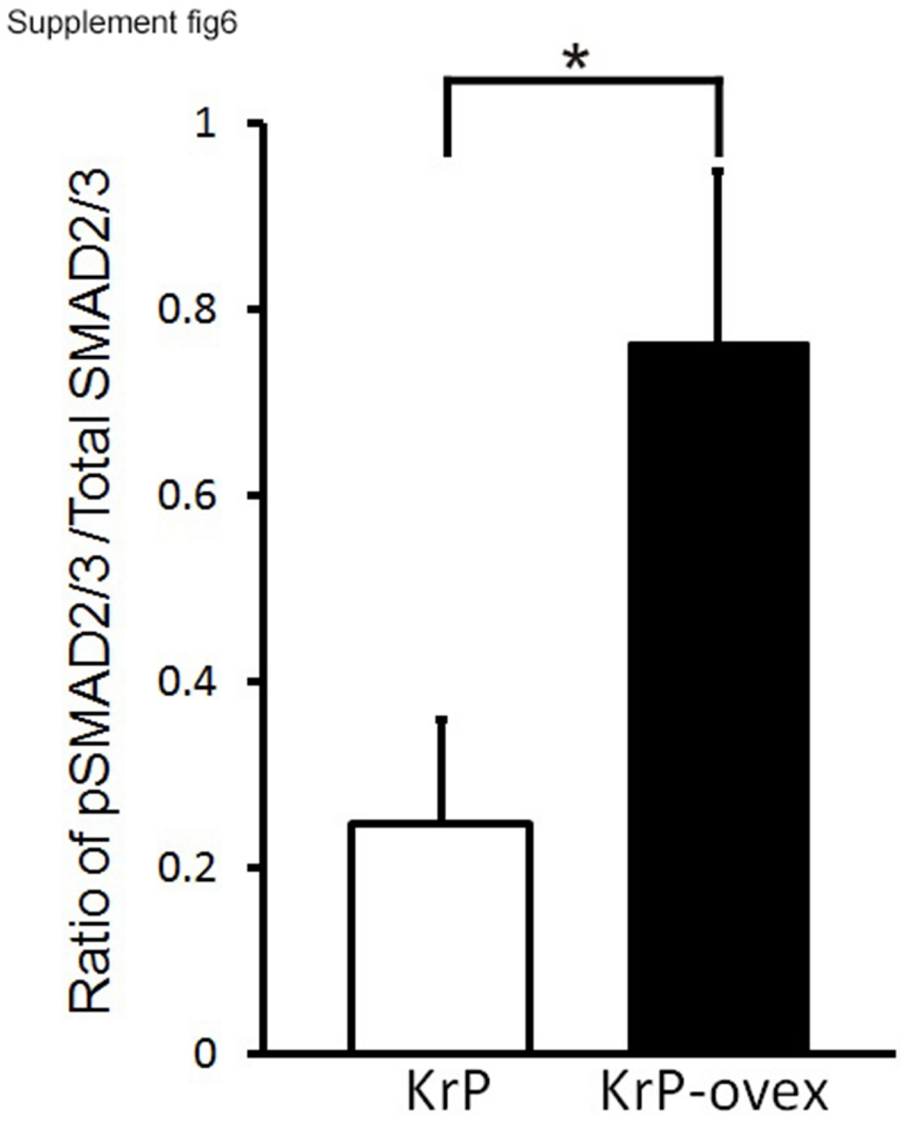

Supplemental Figure S6. Densitometry of pSmad2/3 *vs.* Smad2/3. Western blot shown in Fig. 6H was analyzed using imageJ to determine each band density. A ratio of pSmad2/3 *vs.* total Smad2/3 was calculated for KrP and ovexed KrP mice samples. Each bar represents the average ±s.d. of the triplicate samples blotted together. Extracts were evaluated two times in this manner with similar results. *P < 0.05.

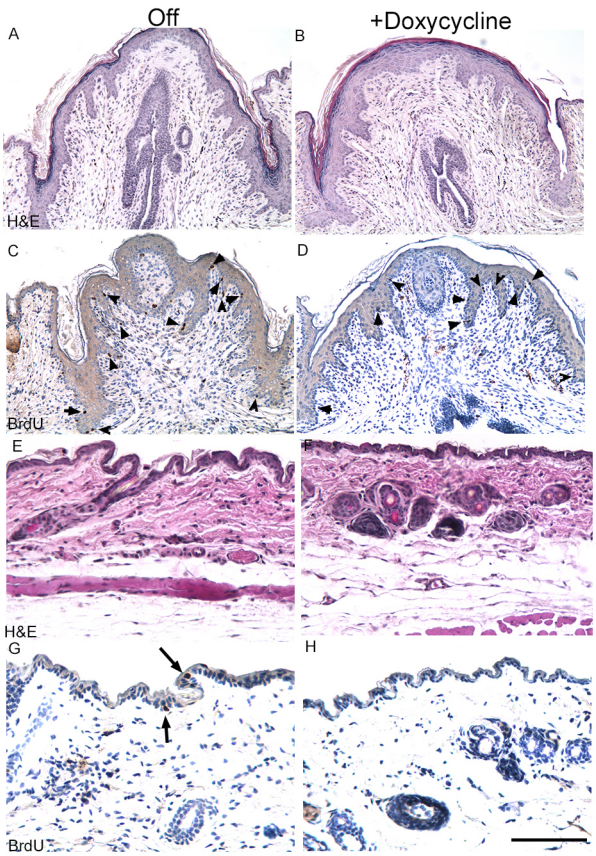

Supplement fig7

Supplemental Figure S7. Overexpression of TGFβ1 in the epidermis. Six-week-old *K14-rTA/tetO-TGF β 1* virgin mice were either placed on doxycycline chow or control chow for 3-weeks, injected with BrdU and harvested. Number 4 and 5 nipples as well as non-nipple skin samples were processed for H&E and BrdU staining. **A, C, E** and **G** sections are from untreated controls and **B, D, F** and **H** from doxycycline treated animals. Nipple samples are **A-D** and ventral skin samples are **E-H.** Scale bar: 190 μm in A-D, 380 μm in E-H. Changes in the ventral epidermis of the TGFβ1 overexpressing mice were readily apparent in that portions of it pealed off during hair removal. Treatment of WT C57BL/6 mice with doxycycline chow failed to produce any detectable changes in the nipple or epidermis (not shown).

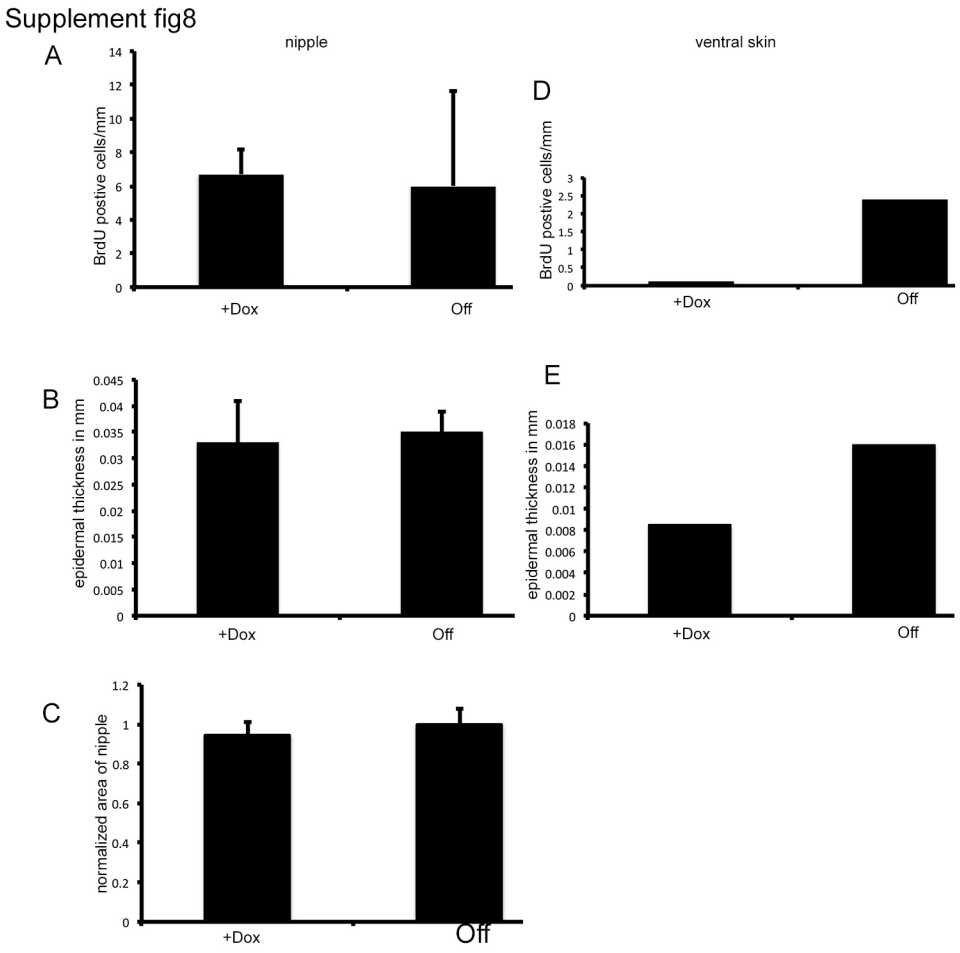

Supplemental Figure S8. BrdU analysis. Sections of eight nipples were analyzed using imageJ for **(A)** BrdU positive cells per epidermal/dermal junction length; **(B)** nipple epidermal thickness; **(C)** nipple area. No statistically significant differences in any of these parameters were observed between doxycycline treated nipples and those of controls. **(D)** BrdU positive cells per epidermal/dermal junction length and **(E)** epidermal thickness were evaluated for the ventral epidermis of the animals (n=2) and these parameters were markedly reduced in doxycycline treated animals.